Seismic reflectivity, fracturing and stress field data from the FFC-1 exploratory geothermal project in SW Skåne, Sweden

Christopher Juhlin [a,*], Mikael Erlström [b,c], Björn Lund [a], Jan-Erik Rosberg [d]

[a] *Department of Earth Sciences, Uppsala University, Villavägen 16, Uppsala 752 36, Sweden*
[b] *Geological Survey of Sweden, Kiliansgatan 10, Lund 223 50, Sweden*
[c] *Department of Geology, Lund University, Sölvegatan 12, Lund 223 62, Sweden*
[d] *Engineering Geology, Faculty of Engineering, Lund University, Box 118, Lund 221 00, Sweden*

ABSTRACT

Enhanced geothermal systems (EGS) are a potential heat source in many parts of the world, even in locations where the temperature gradient is relatively low. We present here an integrated study of reflection seismic data, borehole logs and seismicity analysis performed in conjunction with a geothermal exploratory project operated by E.ON in Malmö, Sweden. In 2020, the pre-existing 2.1 km deep FFC-1 borehole through the sedimentary cover was deepened into the crystalline basement to about 3.1 km vertical depth. Combined interpretation of the reflection seismic data and geophysical wireline logs show that most of the reflectivity in the Precambrian basement is likely generated by lenses of mafic amphibolite embedded in a felsic gneissic matrix. The general structural bedding and foliation is gently dipping to sub-horizontal, similar to other locations in southwest Sweden. Fracture frequency is relatively high in the crystalline rock mass, with heavy fracturing in the upper-most part of the crystalline basement, obscuring a clear reflection from the top of the Precambrian. Highly fractured and hydraulically conductive intervals are also found between 2,562 and 2,695 m based on a temperature drop and the interpretation of the geophysical data. Open fractures, both natural and induced, have a clear N–S orientation, contrasting with the expected NW–SE direction based on the orientation of the Sorgenfrei-Tornquist Zone and earthquake fault plane solutions to the north. This difference may be partly explained by local variations in the stress field near the FFC-1 borehole and vairations in the stress field with depth. Despite this, the data from the FFC-1 well provide novel and unique information on the complex physical state of the crystalline basement on the margin of the Fennoscandian Shield, which further addresses the need for obtaining in-situ stress data to fully understand the local stress field prior to any stimulation. A temperature of 84°C measured at 3 km depth indicates that a desired EGS temperature of 120–140°C may be reached at 5–6 km depth, assuming a temperature gradient of about 20°C. If the relatively high fracture frequency and occurrence of fracture zones down to 3.1 km are also present at these target depths, then the FFC-1 location may be suitable for heat extraction if the rock mass is properly characterized before stimulation.

1. Introduction

Extraction of deep geothermal energy in Sweden was proposed as early as the 1970s (Bjelm et al., 1977; Eriksson et al., 1978; Bjelm et al., 1979; Bjelm and Persson, 1981). Already then, two options were considered: (1) warm water aquifers in the sedimentary rocks of southern Sweden and (2) areas of higher heat flow in the pervasive Precambrian crystalline shield rocks. In the latter case, locations with deep natural fracture zones would be preferred for heat extraction. Later compilations (e.g. Näslund et al., 2005; Veikkolainen et al., 2017)

confirmed that heat flow (and temperature gradients) may vary significantly throughout the crystalline rock of Sweden. Temperature gradients of 30°C/km have been noted in central Sweden (Muhamad et al., 2015), although gradients between 15 and 20°C/km are most common. A few exploratory wells for heat extraction, and in some cases circulation tests, have been made in Sweden. Most notable are the Fjällbacka project in the radiogenic Bohus granite of western Sweden (Wallroth et al., 1999), the drilling into an impact crater east of Stockholm (Henkel et al., 2005) and the deep drilling (3.7 km) into the Romeleåsen Fault Zone in southern Sweden (Rosberg and Erlström, 2019). None of

these projects resulted in any commercial heat extraction. The only commercial larger scale geothermal heat production plant in Sweden utilizes low-temperature sedimentary aquifers at about 400 m to 800 m depth and is located in Lund, close to Malmö, feeding heat into the district heating network via heat pumps (e.g. Bjelm and Alm, 2010). Aside from the above-mentioned studies there has been extensive research on fractures and fracture systems in the crystalline bedrock of Sweden in conjunction with research on the storage of spent nuclear fuel (e.g. Stephens et al., 2015).

The St1 project in Finland (Kukkonen and Pentti, 2021) renewed interest in deep heat extraction in the Precambrian of the Fennoscandian Shield. Two boreholes were drilled to 6.2 and 6.4 km measured depth (MD) with the goal to circulate fluid between them and extract heat that could be fed into the Espoo city district heating system. Hydraulic stimulation was performed between the boreholes. As of now, no heat has yet been extracted from the system, but tests are ongoing. The advantage of the St1 concept is that boreholes can be drilled next to existing district heating systems in populated areas so that once the initial drilling and stimulation investment are made there is little additional cost for the energy source. This assumes that drilling costs are reasonable, and that stimulation is feasible without significant induced seismicity.

Even though there is no deep (> 1 km) heat extraction currently in Sweden, there is significant use of low temperature, shallow geothermal energy systems utilizing ground source heat pumps (Gehlin et al., 2020). These are generally connected to single family homes for space and hot water heating, but recently the number of larger residential and non-residential shallow geothermal energy systems has increased significantly. As of 2019, about 17.1 TWh of heat is produced annually from these shallow single-family and larger systems. An additional c. 50 TWh of heat was produced by district heating systems in 2019 (www. scb.se). These figures may be compared to a total energy consumption in Sweden of about 550 TWh in 2018 (www.energimyndigheten.se) and the c. 19.8 TWh electricity produced by wind in 2019. These numbers suggest that deep heat extraction may be able to contribute significantly to Sweden's future energy needs if technological and geological challenges can be overcome. Aside from reductions in drilling costs, these challenges include how to best stimulate the crystalline bedrock to increase permeability, development of optimum monitoring methods of induced seismicity and how to better predict geological conditions at depth, in particular the presence of fractures. Geological aspects of particular importance include (1) characterizing site specific geological conditions in the crystalline basement, (2) evaluating the seismic noise levels to determine what magnitude seismic events can be detected and with what instrumentation, and (3), based on point (2), understanding the seismic risk in an area during stimulation.

Based on the initiative of St1 and the need to replace existing heating systems, E.ON decided to explore the possibility for heat extraction from the Precambrian crystalline rock in the Malmö harbor area in southern Sweden. E.ON's interest was to investigate the prerequisite for establishing a 40–50 thermal MW Enhanced Geothermal System (EGS) plant using a classical doublet. Such a plant would cover 10% of the district heating demand in the city of Malmö. Initial focus has been in the same area as two exploration wells in the sedimentary strata, FFC-1 and FFC-2, were drilled and completed in 2002 and 2003, respectively. At that time, the aim was to explore if the deep-seated sandstone reservoirs within the Mesozoic successions were suitable for geothermal heat production and drilling was stopped after reaching the top of the crystalline basement at around 2.1 km depth. Geothermal exploration of these Mesozoic sandstone aquifers was halted in 2004 due to the project not being economically feasible for district heating in Malmö. However, the wells were not plugged and abandoned and in 2020, after a couple of years of feasibility studies regarding the EGS potential in Malmö, it was decided to re-enter one of the wells, FFC-1, and deepen it 2 km into the crystalline basement to a total depth of 4 km. It was cost efficient to use the old well, because the around 2.1 km thick sedimentary succession on top of the crystalline basement was already drilled and cased. In addition, a geophone array was installed in the other well, FFC-2, for seismic monitoring while drilling. The seismic monitoring system was expanded with two wells in early 2020, ÖVT-1 and FFC-3, both drilled and completed in the sedimentary succession, to 792 m and 767 m depth, respectively. The aim with re-entering the FFC-1 well was to gain increased knowledge about the crystalline basement below 2.1 km depth as a step in the planning of a full-scale EGS-plant. In the region there is only one borehole that provides geological information about the deep basement and its physical properties down to around 3.7 km and that is the DGE-1 well in Lund (see Rosberg and Erlström, 2019), about 20 km north-east of Malmö (Fig. 1). The lack of data from the deep crystalline basement was a strong motivation for further exploratory drilling. Deepening of the FFC-1 well had the following objectives for data and information gathering:

- Information about drilling performance using air-percussion drilling, as well as gaining experience of deep drilling in the crystalline basement to reduce cost for upcoming projects.
- Evaluating the applicability of seismic monitoring during the drilling operation.
- Information about the rock types, including properties for characterization of the rock mass.
- Data required for interpreting and verifying the surface seismic measurements.
- Data on fracture intensity and characteristics, which are of crucial importance when designing and constructing an EGS-system. If a significant amount of open fractures are present water will flow naturally between boreholes. If only closed fractures are present then these will influence the stimulation process.
- Data on in-situ geophysical, thermal, hydraulic, and mechanical properties. Input data required for the modelling of a full-scale EGS-system.

The deepening of the FFC-1 well started in late June 2020 and ended after two months at 3,133 m MD. The initial plan to drill to 4 km using air-percussion drilling proved infeasible. Several attempts were made, but due to a too high inflow of formation fluid this drilling technique had to be discontinued. Conventional rotary drilling was used for the subsequent drilling and the target depth was changed to around 3 km, a depth considered suitable for post-drilling seismic investigations in the borehole and for obtaining new information about the upper 1 km of the crystalline basement. Data from the crystalline basement section acquired during and after the drilling are compiled in Rosberg and Erlström (2021), as is an overview of the drilling operation.

In this paper we present an overview of the most relevant geophysical and geological studies performed at Malmö harbor in association with the extended drilling of the FFC-1 borehole. These include reflection seismic data, geological and geophysical logs, seismicity studies and measurements on rock samples, with a focus on the deeper crystalline section of the borehole. We show that reflections on the seismic data from the Precambrian are most likely generated by gently dipping mafic amphibolite lenses within a dominant felsic gneissic rock mass. Based on seismicity analyses in the general area and on monitoring at the site we frame the location into its tectonic setting and its relation to the stress regime. We also discuss the seismic hazard and the potential for fault reactivation. Finally, we speculate on how the results from this study are relevant for the prospects of exploiting deep geothermal energy in Sweden and how the integration of surface seismic data with the borehole results may be useful for interpreting seismic data over Precambrian bedrock in general.

2. Geological setting

FFC-1 was drilled in southwest Skåne, the eastern marginal part of the Danish Basin. The Precambrian crystalline basement is in FFC-1
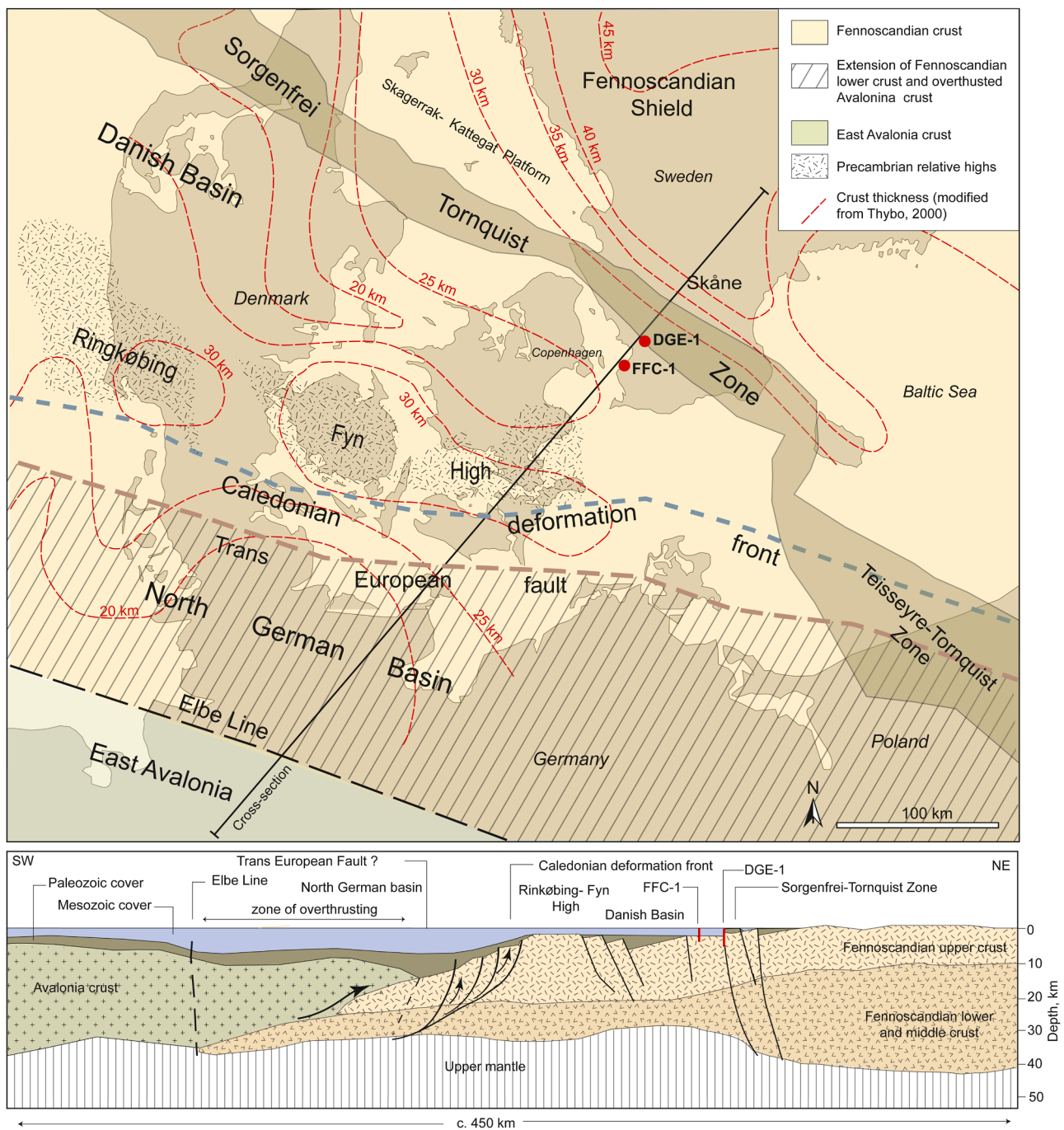
Fig. 1. Schematic map and cross section showing the crustal framework of north Germany, Denmark and south Sweden, and the locations of the FFC-1 and DGE-1 wells.

covered by a 2,100 m thick succession of Mesozoic strata. These include Triassic arkose and claystone followed by Lower Cretaceous–Lower Jurassic sandstone and claystone, and a 1,600 m thick Upper Cretaceous limestone-dominated sequence. The crystalline bedrock beneath the sedimentary cover represents the southwest margin of the Fennoscandian Shield and the transition from older stable cratonic areas to the northeast to younger metastable geological provinces to the south. To the south and southwest, the Fennoscandian Shield is characterized by decreasing crustal thickness and a successively thicker cover of sedimentary strata. The crust is believed to be in the range of 30 km thick in southwest Skåne and the FFC-1 site, significantly thinner in comparison to >40 km for the interior parts of the shield (Balling, 1995; Thybo, 2000; Fig. 1). Fennoscandian crust is interpreted to continue into

northwest Germany beneath a zone of overthrusted Avalonina crust. The outer limit is believed to be located somewhere between the inferred Trans European Fault and the Elbe Line in north Germany (c.f. EUGE-NO-S Working Group, 1988; Thybo, 1990; Tanner and Messner, 1996; Lyngsie and Thybo, 2007; Fig. 1). The southwestern part of the Fennoscandian Shield, between the Sorgenfrei-Tornquist Zone (STZ) and the Caledonian deformation front is, furthermore, weakened by a fan of primarily northwest–southeast striking faults and faults zones formed during Caledonian, Variscan and Alpine deformation phases (Figs. 1 and 2). The most significant one being the STZ that has been repeatedly active during the Phanerozoic tectonic events (Erlström, 2020). Another significant feature is the Ringkøbing-Fyn High which consists of a series of relatively shallow lying crystalline basement highs that separate the
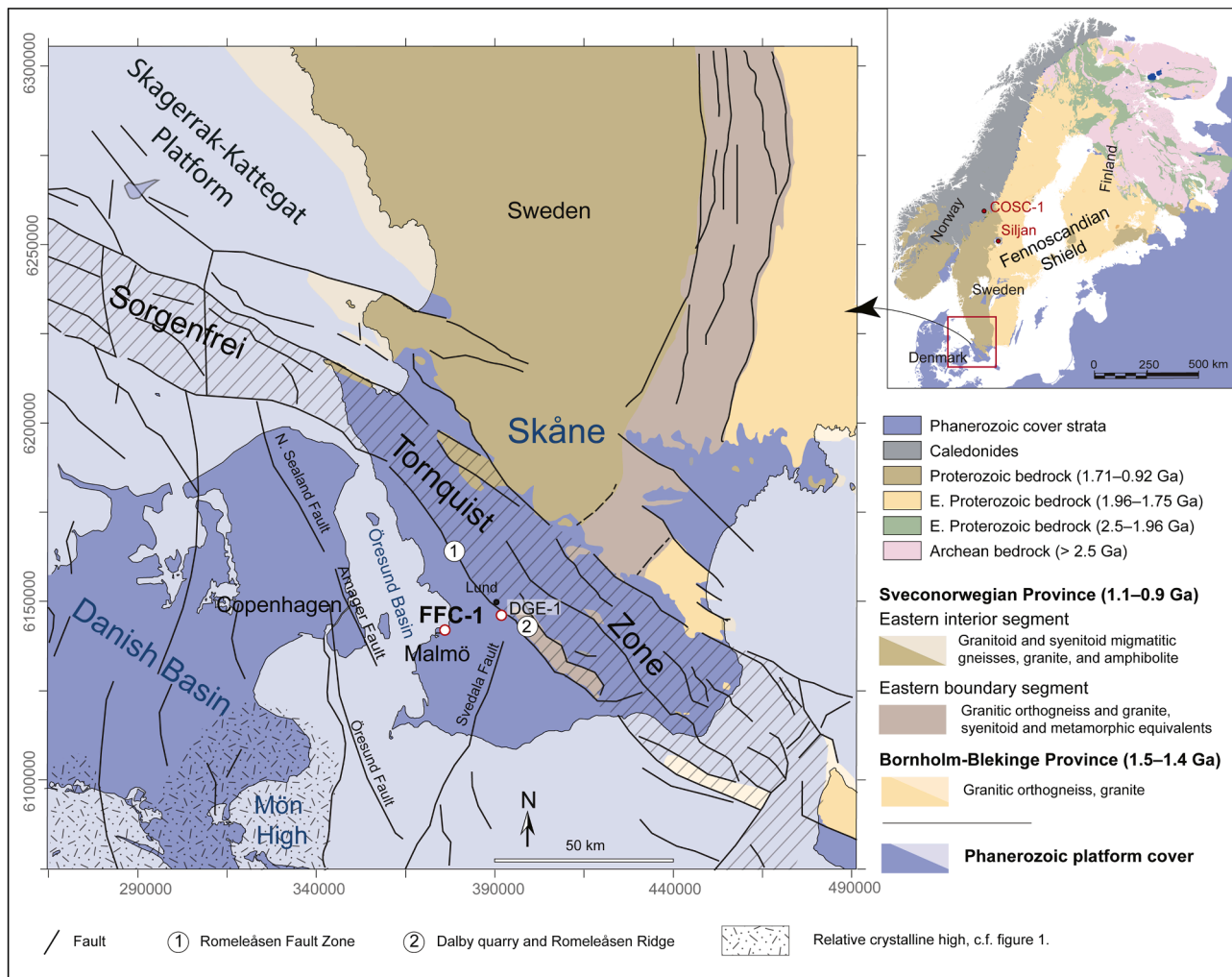
Fig. 2. Schematic map showing the FFC-1 site and the regional geological framework. Coordinates in SWEREF 99 (standard Swedish system and given in m). Figure based on Rosberg and Erlström (2021). Inset shows the locations of the Siljan and COSC-1 boreholes.

Danish and North German basins (Fig. 1).

The Fennoscandian crust in southwest Sweden is composed of the Sveconorwegian gneiss-dominated province (Fig. 2). The original rocks are c. 1.8–1.7 Ga old granitoid rocks, which were metamorphosed 1.1–0.9 Ga ago (Ulmius et al., 2018; Stephens and Wahlgren, 2020). The present-day exposed rocks represent original deformation depths of up to several tens of kilometres in the crust, thus, associated with the deeper roots of a c. one billion-year-old eroded mountain chain.

Prior to re-entering and deepening the FFC-1 well there were only a few scattered observations on the composition of the crystalline basement beneath the roughly two-kilometre-thick succession of Triassic–Paleogene strata on top of the crystalline basement in SW Skåne. These came primarily from oil and gas prospecting wells touching or reaching only a few meters into the basement (Sivhed et al., 1999). The main source of neighbouring information on the crystalline bedrock had so far been the 3.7 km deep DGE-1 borehole in the Romeleåsen Fault Zone and outcrops on the Romeleåsen Ridge, c. 20 km northeast of the FFC-1 site (Sivhed et al., 1999; Erlström et al., 2004; Rosberg and Erlström, 2019). These observations show a crystalline basement with a complex mixture of Precambrian inherited tectonic signatures and Caledonian, Variscan and Alpine orogenic deformation phases during the Phanerozoic break-up of the south-western margin of the Fennoscandian Shield (Libouriussen et al., 1987; EUGENO working group, 1988; Erlström et al., 1997; Thybo, 2000; Erlström, 2020). These younger tectonic events included fault reactivation and wrench

tectonics, which have given a rock mass highly intersected by fractures, joints, fissures, and veins (cf. Bergerat et al., 2007).

Most of the younger tectonic movements are manifested by the NW–SE striking STZ. Fault reactivation, repeated strike-slip displacements and inversion tectonics were characteristic events in the evolution of the STZ (Erlström et al., 1997; Erlström, 2020). Overall, the Phanerozoic faulting and fracturing are dominated by NW–SE, N–S and NNE–SSW oriented faults and fractures (Bergerat et al., 2007). Dextral strike-slip movements were a significant component in the tectonic regime during both the extensional and compressional phases centered around the STZ in Variscan and Alpine times (Blundell et al., 1992; Thomas and Deeks, 1994; Thybo, 1997; Mogensen, 1994, 1995; Erlström and Sivhed, 2001). Sinistral movements in Skåne have been documented by Sivhed (1991). However, there are few observations on the actual aggregate lateral offset, but Sivhed (1991) and Mogensen (1994) judge these to be less than 20 km. A set of NNW–SSE and NNE–SSW oriented Triassic extension faults are found to the west of the FFC-1 site, including the Öresund, Amager and North Sealand faults, and the Svedala Fault to the east (Fig. 2). These have played a major role in the formation of the half grabens in the Öresund Basin (Erlström et al., 2018).

A major positive Bouguer gravity anomaly coinciding with the STZ is interpreted to be caused by high-density rocks in the deeper crust beneath the zone. These were likely emplaced during Permo-Carboniferous Variscan rifting and coeval with the intrusion of a

magmatic dolerite dyke swarm across Skåne (cf. Balling, 1990; Thybo, 2000; Erlström, 2020). These up to c. 50 m wide steeply dipping NW-oriented dolerite dykes are significant components of the bedrock and comprise up to c. 10% of the total rock mass in the STZ in Skåne.

Thus, the FFC-1 well is placed in a geological setting which is believed to consist not only of inherited Precambrian structures and relatively thin crust, but also a series of relatively young brittle deformation features that sets the structural and thermal framework prerequisites for EGS. When evaluating the stresses and fracturing in the crystalline basement one also must consider that FFC-1 is located outside the STZ, in the Danish Basin with km-thick successions of sedimentary strata covering the basement (Erlström, 2020).

3. Available data used for this study

3.1. Reflection seismic data

During the autumn of 2000, about 29 km of land seismic data were acquired by THOR Gmbh (Kiel) in the northern part of the Malmö area (Fig. 3) along six lines (MVL01/05, 02/07, 03, 04, 06 and 08) using a vibroseis source with the goal to cross, as much as possible, existing faults and connect to older existing offshore profiles. The data were acquired along crooked lines with simultaneous recording along other lines while some of the lines were being shot. The seismic data are generally of good quality and where the fold is high it is possible to obtain good images. Low fold areas away from the acquisition lines are more problematic, but even at some of those locations it was possible to obtain good images. Acquisition parameters are presented in Table 1.

Original processing of the data was performed by TEEC (https://teec. de) from Hannover with a focus on the sedimentary section. Later reprocessing was done at Uppsala University to map horizons within the sedimentary section in 3D. In 2017 the data were again reprocessed at Uppsala University to enhance the images in the Precambrian section down to 6–7 km (Table 2). We focus here on the western part of line MVL01/05 and line MVL03 which cross one another near the FFC-1 borehole (Fig. 3).

Processing followed a standard sequence (Table 2) with choice of filters and velocities having the greatest influence on the final result. Good statics were obtained given the strong reflectivity in the sedimentary section for maximizing the solution. Line MVL01/05 is quite

Table 1
Seismic acquisition parameters.

Crew	THOR
Acquisition dates	27 Nov 2000 – 02 Dec 2000
Recording system	ARAM24NT S/N 24b-46
Sampling interval	2 ms
Record length	6 s
Number of channels (nominal)	240
Geophones	12×10 Hz group at 2 m spacing
Receiver spacing	25 m
Source	Pelton ADVII Vibroseis
Sweep	Non-linear log, 10000 ms
Start/End frequency	10/100 Hz
Source spacing	50 m
Nominal fold	60

Table 2
Seismic processing steps.

Step	Process
1	Read SEGY data from Exabyte tape
2	Extract geometry from SPS files
3	Bin data into 12.5 m CDP bins
4	Add geometry to trace headers
5	Scale traces by t^2
6	Phase shift -90 degrees
7	Spiking deconvolution: whitening 0.1%, filter length 160 ms
8	Bandpass filter: 15–25–90–120 Hz 0–1400 ms, 5–15–70–100 Hz 1600–3000 ms
9	Phase shift +90 degrees
10	Refraction static corrections: datum – 0 m
11	Spectral equalization 20–40–100v120 Hz
12	Residual static corrections
13	AGC: 200 ms
14	NMO
15	Stack
16	FX-Decon: 40 traces, 120 ms window
17	Finite difference migration: 85% of RMS stacking velocity used
18	Depth conversion: 95% of 1D velocity at FFC-1 well used

crooked in parts, both regarding the source locations and the receiver locations. Therefore, the data were projected onto a straight Common Depth Point (CDP) line to simplify interpretation. Figs. 4a and b show results from the processing of the two lines down to 3 s. The sedimentary
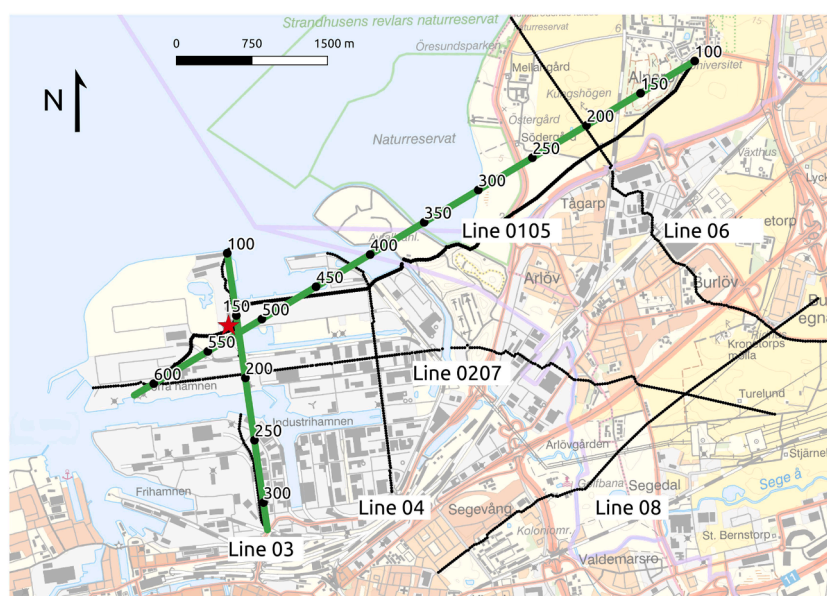

Fig. 3. Location of the seismic profiles (black lines) acquired in the Malmö area in 2000. Lines 01/05 and 03 are presented in this paper and their corresponding CDP (Common Depth Point) stacking lines are shown in green with CDP numbers labeled. Red star marks the location of the wellhead of the FFC-1 borehole.
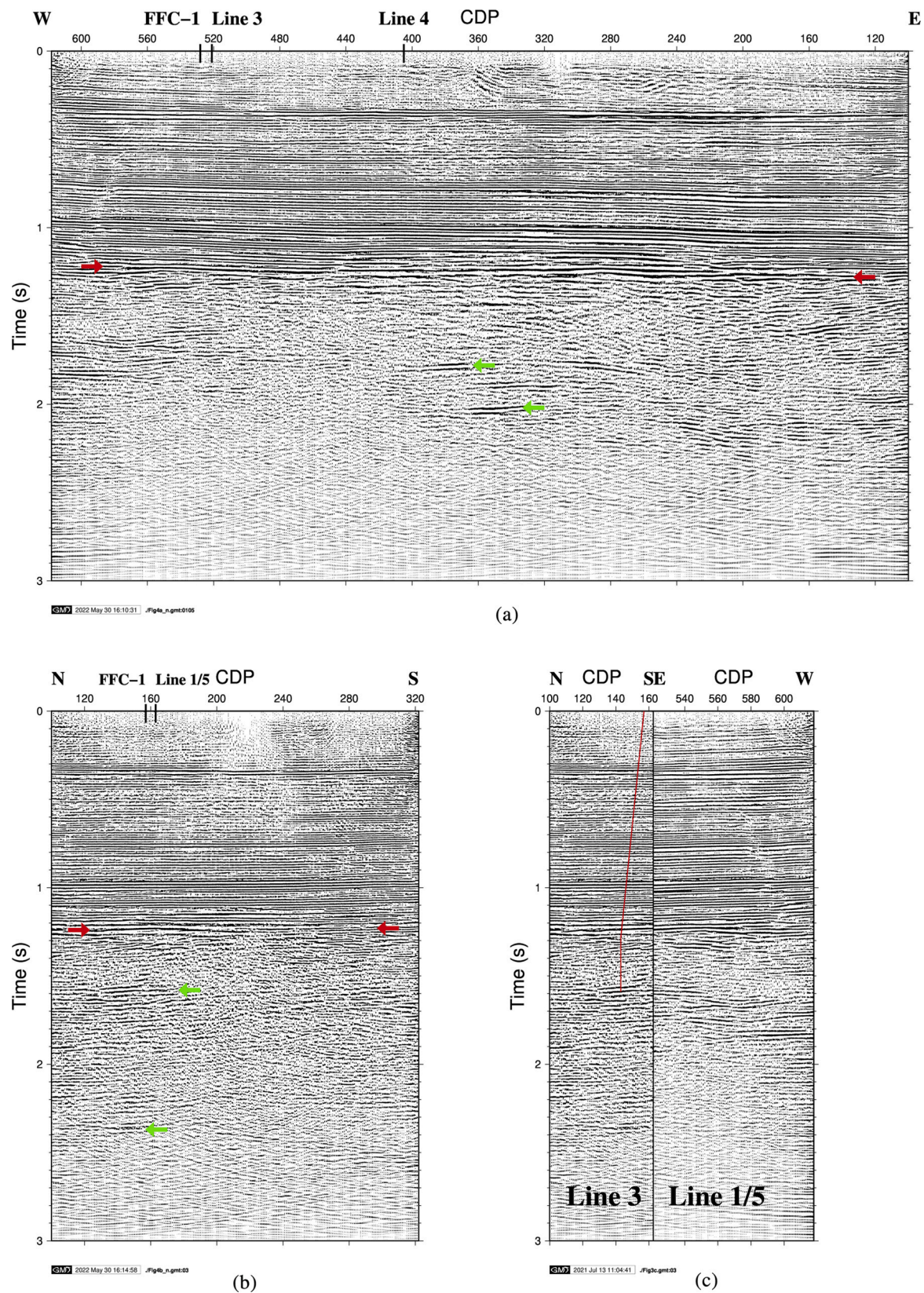
(a)

(b)

(c)

Fig. 4. (Top - a) Results from reflection seismic processing MVL01/05. Interpreted base of the sedimentary section is shown by red arrows. Examples of interpreted amphibolite lenses are shown by green arrows. Vertical to horizontal scale is approximately 1 in the sedimentary section and 0.5 in the crystalline basement. (Bottom left - b) Results from reflection seismic processing MVL03. Interpreted base of the sedimentary section is shown by red arrows. Examples of interpreted amphibolite lenses are shown by green arrows. Vertical to horizontal scale is approximately 1 in the sedimentary section and 0.5 in the crystalline basement. (Bottom right - c) Results from reflection seismic processing MVL03 and MVL01/05 merged where they cross and looking from the northwest. Red line marks approximate trajectory of the FFC-1 borehole relative to MVL03.

section is clearly imaged down to about 1.25 s. Numerous discontinuous to semi-continuous reflections are observed at later times. No distinct top of basement reflection is observed. By merging the two lines where they cross one another (Fig. 4c) we note that there is continuity across the sections below 1.25 s, implying that the reflections from below the base of the sedimentary section are sub-horizontal and indeed originate in the Precambrian basement, at least near the borehole. Reflections from line MVL04 (not presented here) below 1.25 s also have a sub-horizontal orientation, implying that the deeper reflections along MVL01/05 at around CDP 400 are also originating from sub-horizontal structures in the Precambrian basement. We will show later that the most pronounced reflections are generated where thicker amphibolite

bodies are present.

3.2. Borehole data

During the deepening of the FFC-1 borehole in 2020 no cores were recovered, but cuttings were collected from the crystalline rock section. Wire-line logging of the crystalline section was performed by Weatherford and included surveys with Gamma Ray, Spectral Gamma Ray, Photo-Density, Compact Cross-Dipole Sonic (CXD), Slim Compact Micro-imager (SCMI), including multi-arm Caliper and borehole deviation tools (Ciuperca et al., 2021). A temperature sensor was included in the plans, but no high-resolution temperature tool was run in the
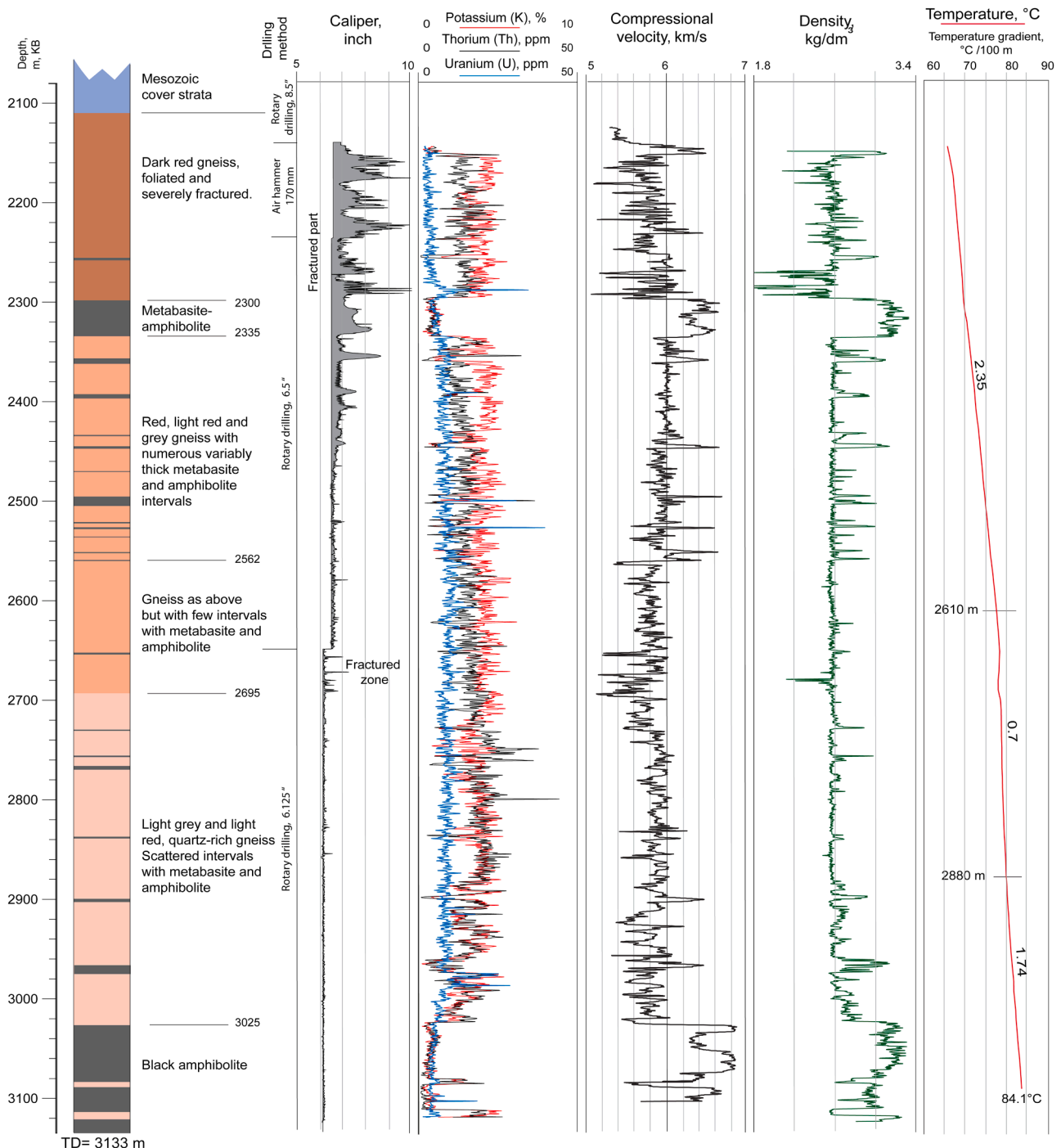

Fig. 5. FFC-1 composite log with interpreted rock succession, Caliper, Spectral Gamma Ray, CMX derived compressional velocity, density and temperature. Depths are measured depth (MD).

borehole due to technical problems.

The description of the crystalline bedrock succession and fracturing is largely based on the compilations presented in Rosberg and Erlström (2021) and Ciuperca et al. (2021).

3.2.1. Rock types

The significant difference in potassium/thorium content and density for the two dominating mafic and felsic rock types is clearly depicted by the Spectral Gamma Ray and the density logs (Fig. 5). Combined, these logs allow correlation of the collected cuttings to defined depths for these two main rock suites.

Most of the penetrated rock mass in FFC-1 is composed of felsic rocks, dominated by quartz, feldspar, and minor amounts of mica and hornblende. The mica is dominated by biotite which mainly occurs aligned along the foliation of the rock. The deeper red felsic rocks are dominated by potassium feldspars while the light red and grey varieties are richer in plagioclase and quartz. Muscovite is predominantly found in the greyish relatively quartz-rich felsic rocks below 2,700 m. Scattered intervals enriched with muscovite are also identified at 2,630–2,640 m, 2,756–2,786 m and 2,835–2,841 m. These various types of light red, grey and dark red gneiss with either granitic or granitoid origin comprise about 80% of the rock mass. The shifts between the gneiss varieties, except for the upper one, down to 2,300 m, are ambiguous and only weakly portrayed as small shifts in the characteristics of the cuttings and the Spectral Gamma Ray log signature (Fig. 5). In general, the gneisses below 2,300 m depth are less foliated, banded, and relatively quartz rich.

The second dominating rock type in FFC-1 is dark grey–black mafic amphibolite–metabasite. This rock type is dominated by hornblende, biotite and a varying amount of quartz, plagioclase, and garnet. Only traces of potassium feldspars have been observed. These rocks are often thinly interlayered with biotite gneiss and can be classified as foliated amphibolite-gneiss. In total, the mafic rocks comprise about 20% of the rock succession and occur both as thick bodies in the upper part (2,300–2,335 m) and bottom part (3,025–3,133 m), and as up to meter-thick intervals, likely lenses, or irregular thin bands within the felsic intervals. Worth noting is that there are no observations of NW–SE oriented Permo–Carboniferous dolerite in FFC-1. If the absence in FFC-1 is due to that the well by chance is located between dykes or if this is a significant characteristic for the rock mass is unclear. Since FFC-1 is located to the SW and outside the positive gravity anomaly coinciding with the STZ in central Skåne, SW Kattegat, and Bornholm this could explain the observed absence of dolerite.

There is a significant difference in density between the mafic and felsic rock types. The gneiss densities are relatively constant at around 2.6 g/cm^3 while the metabasite/amphibolite have densities ranging between 2.9 and 3.2 g/cm^3 (Fig. 5). Complementary analyses on cuttings material, performed by RWTH Aachen (Klitzsch and Ahrensmeier, 2021), verify similar density values for the two rock types (Fig. 6). Comparable densities are also documented on outcrop samples of gneiss and amphibolite on the Romeleåsen Ridge (Rosberg and Erlström, 2021). The density measurements on cuttings and outcrops verify that the felsic rocks have densities consistent with what the density log show, i.e. densities around 2.6 g/cm^3. Note that the log response often gives slightly higher values for the amphibolite–metabasite in comparison to the 2.9–3.0 g/cm^3 which is the result from the laboratory measurements (cf. Fig. 5).

3.2.2. Fractures

For the upper part of the crystalline bedrock the Caliper log shows relatively poor borehole conditions with several sections showing an increased caliper reading (c.f. Caliper log in Fig. 5). This is caused by the presence of highly fractured rock sections, which during the percussion drilling were coupled with high water inflow (Rosberg and Erlström, 2021). The increased hole size in these sections have resulted in partly erratic SCMI and CXD data down to c. 2,366 m. Below this depth there were no significant borehole related quality issues that affected the logging results. The fracture data from the SCMI and CXD logs presented here are, thus, based on the data below 2,366 m.

The SCMI tool was run as a dual setup with 2•8 pads covering c. 50% of the borehole wall, which provided good imaging of the fracturing. Besides providing coherent data on frequency, orientation, and direction of the fractures below 2,366 m depth the SCMI data verify that there is a zone with increased fracturing between 2,562 m and 2,695 m. This zone is also characterized by less dense sections and relatively lower velocities in the density and CXD logs (Fig. 5).

A total of 995 fractures have been identified as sinusoid traces in the SCMI data between 2,366 m and 3,106 m depth. The identified fractures include a range of fully electrically conductive to fully electrically resistive ones, which are either individual or connected to each other. Of these, approximately 15% are interpreted to be fully conductive and open. The interpreted open fractures included all continuous, electrically conductive features with apparent aperture (Ciuperca et al., 2021). The hydraulic openness of these fractures was not possible to further verify since the high-resolution temperature tool did not pass below a tight section or ledge at c. 2,370 m. Thus, the temperature data come

Rock type: Felsic, light red gneiss, weakly foliated with dark minerals (biotite)
Density: 2.65 g/cm^3 ± 0.02

Rock type: Mafic, dark grey-black metabasite and amphibolite
Density: 2.99 g/cm³ ± 0.03

Fig. 6. Examples of cuttings of a) typical felsic gneiss and b) mafic metabasite and amphibolite.

only from a standard temperature measurement combined with the CXD and SCMI logging. However, the frequent occurrence of soft whitish kaolinite and albite-altered plagioclase in the cuttings in connection with highly fractured intervals indicate to some extent hydraulically active zones where weathering takes place.

Below 2,366 m the fracture frequency is at most 4–6 fractures/m, however most commonly the frequency is below two fractures per meter. The average fracture volumetric density varies between 3.39 and 1.68 m^2/m^3 from the upper to the lower parts of the well (Rosberg and Erlström, 2021). The fracture data are dominated by relatively steeply dipping and N–S oriented fractures. Even if there is a wide range of other directions, the N–S oriented cluster is significant both for the interpreted conductive open fractures and for the other fractures (Fig. 7a and c). The few drilling enhanced (n=30) and induced fractures (6) and two 10 cm short tensile regions (defined as tensile failure in a zone) also coincide with this general orientation (Fig. 7b). A north–south dominant

direction of the open fractures is also corroborated by the alignment of the fast shear wave azimuth (Fig. 7d). The relatively high fracture frequency and fracture volumetric density in the deep crystalline basement observed in the SCMI-data is promising from an EGS-perspective, if similar values can be found at greater depths as well.

3.2.3. Stress indicators

There was no focused borehole stress determination campaign performed in FFC-1. Several logs and measurements taken primarily for other reasons can, however, be used to estimate, or constrain, in-situ stresses. Leak-off tests or formation integrity tests can constrain the magnitude of the minimum principal stress. Failure of the wellbore wall due to stress concentration can be identified in image logs, such as the SCMI-data, and used to estimate directions and magnitudes of the principal stresses. Unfortunately, no leak-off tests or formation integrity tests were performed in FFC-1. The SCMI image data showed no
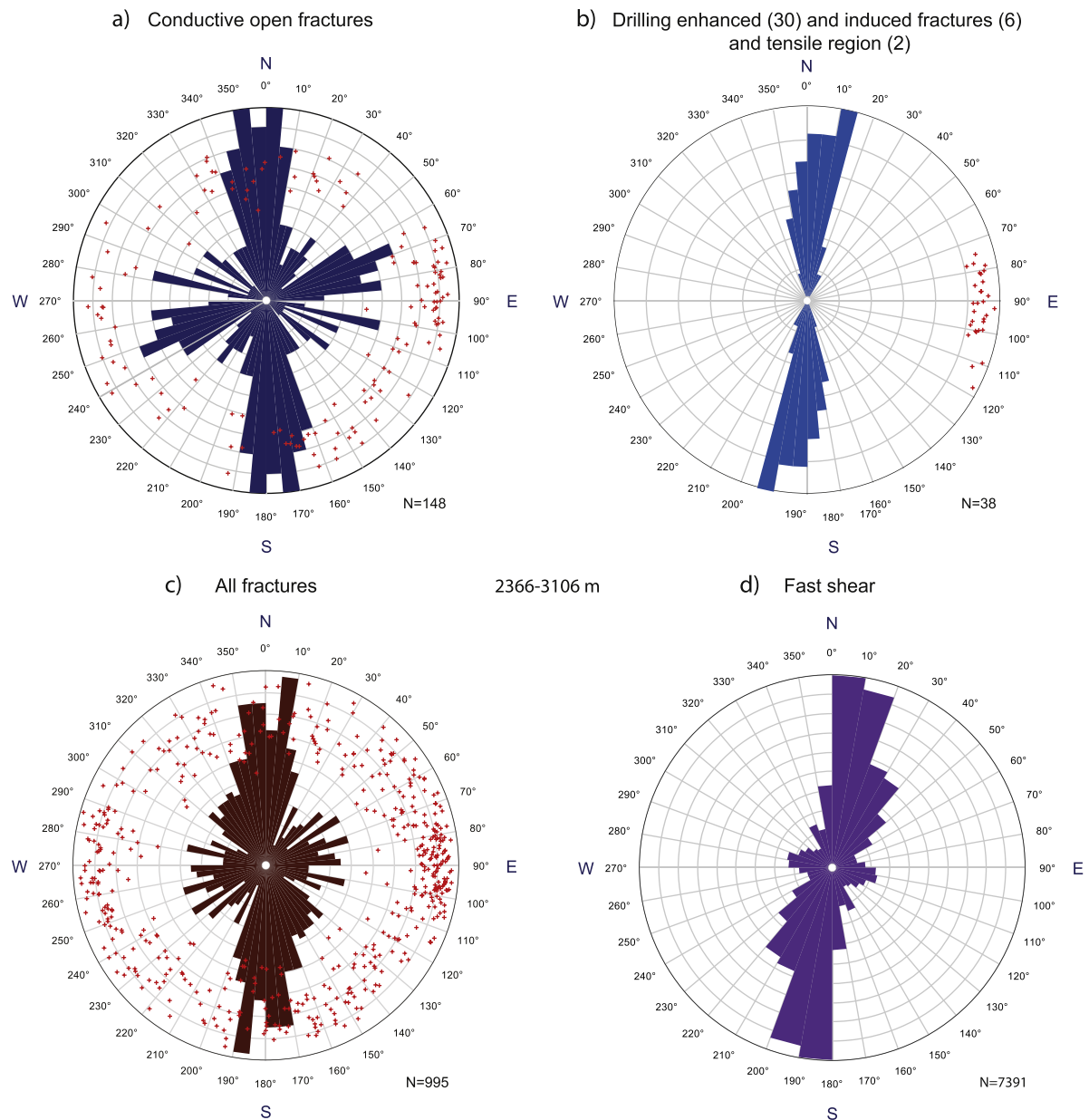

Fig. 7. Combined rose diagrams showing the strike and Schmidt plots (equal area lower hemisphere) showing the dip and dip azimuth of; a) electrically conductive fractures interpreted to be open, b) drilling enhanced and induced tensile fractures, and tensile regions, c) the whole fracture data sets. Figs 7a-c represent data from the SCMI-log. d) Rose diagram of the general alignment of the fast shear azimuth, based on the CXD-log. The plots represent the interval between 2,366 and 3,106 m in FFC-1.

borehole breakouts anywhere in the logged section of the borehole. As noted above, six drilling induced tensile fractures were identified in the SCMI data, two at 2,461.5 – 2,462.9 m and four between 2,522.6 and 2,527.6 m, for a total of 6.5 m, all oriented vertically along the borehole wall in the direction N-2° to 20°E. In addition, two zones of vertical tensile failure were observed at 2,541 m depth, over a length of 4 m at N13° – 23°E. None of these eight tensile features are very clearly imaged. In the SCMI-data there are features identified as drilling enhanced fractures, i.e. natural fractures reopened or aperture enhanced by drilling. These are primarily found in two intervals, 2,507 to 2,542 and 2,792 to 2,825 m, dipping steeply to the west and striking N-15° to 28°E, with an average of N2.4°E. The upper of these intervals is found below a 10 m thick metabasite-dominated interval between 2,495 and 2,505 m, which is characterized by a relatively higher rate-of-penetration, 4–6 m/h. Poor rock conditions are also indicated by the Caliper log in the 2,521–2,528 m interval. These observations appear near the transition interval into more homogeneous gneissic rock, characterized by a less heterogeneous density signature, partly due to fewer intervals with mafic rocks.

The CXD-log shows that the direction of the fast shear wave is NNE–SSW (Fig. 7d), in agreement both with the directions of the drilling induced and enhanced tensile fractures (Fig. 7b) and the general direction of fractures in the borehole (Fig. 7c). Whether the fast shear direction is determined by stress, keeping microfractures open in the NNE–SSW direction, or by the structural fabric is difficult to determine without additional information. The caliper logs have not been analyzed for breakouts as none were visible in the SCMI data.

All data considered, there are very few reliable stress indicators from FFC-1. The fact that the drilling induced tensile fractures are oriented along the borehole axis, and that the borehole is near-vertical, implies that one of the principal stresses is approximately vertical and consequently that the vertical, the maximum horizontal and minimum horizontal stresses are principal stresses. All the tensile regime fractures are expected to form subparallel to the direction of the maximum horizontal stress in a near-vertical borehole and thus indicate that the direction of the maximum horizontal stress at about 2,500 m depth is N–S to NNE–SSW. The lack of leak-off or formation integrity tests, the lack of borehole breakouts, and the scarcity of induced tensile fractures, makes the determination of stress directions uncertain at best, and stress magnitude determination impossible in FFC-1. As the World Stress Map (WSM) quality ranking scheme does not consider drilling enhanced fractures, the tensile fracture data only give a WSM ranking of "D: Questionable S_H orientation". The data indicate that the differential stresses in most of the crystalline section of the borehole are not large enough compared to the strength of the in-situ rock to cause failure.

The simultaneous lack of breakouts and induced tensile fractures does put some constraints on the difference between the maximum and minimum horizontal stress magnitudes. The stress concentration resulting from drilling the borehole makes the circumferential, or hoop, stress, $\sigma_{\theta\theta}$, at the wellbore wall vary significantly over the 90 degrees from the direction of the maximum horizontal stress, S_{Hmax}, to the direction of the minimum horizontal stress, S_{hmin}, (e.g. Zoback, 2007):

$$\sigma_{\theta\theta}^{max} - \sigma_{\theta\theta}^{min} = 4(S_{Hmax} - S_{hmin})$$

Following Zoback (2007) and assuming a Mohr-Coulomb failure criterion for the formation of borehole breakouts we find that if there are no breakouts and no drilling induced tensile failure the maximum horizontal stress is limited by

$$S_{Hmax} \leq S_{hmin} + \frac{1}{4}(C_0 + q\Delta P - T)$$

$$q = \left(\sqrt{\mu_i^2 + 1} + \mu_i\right)^2$$

where C_0 is the uniaxial compressive stress, ΔP the difference between the pore pressure and the borehole fluid pressure, T is the tensile

strength (a negative quantity) and μ_i the coefficient of internal friction. Unfortunately, there are no measurements of C_0 from FFC-1.

A dedicated stress measurement campaign in FFC-1 would be necessary to determine both directions and magnitudes of the in-situ stresses. Such a campaign would preferably also include coring with associated strength measurements.

3.2.4. Temperature

A temperature gradient of 2.35°C/100 m was noted in the crystalline basement above 2,562 m (Fig. 5). As noted above, between 2,562 m and 2,695 m there is a zone with increased fracturing. This zone is hydraulically active, which results in a significantly lower temperature gradient over the actual interval as well as affecting the temperature profile below the zone. In the zone the gradient is 0.7°C/100 m and below the zone it is 1.74°C/100 m (Ciuperca et al., 2021; Fig. 5). A bottom hole temperature of 84.1°C was recorded at 3,100 m.

3.3. Seismicity in the Malmö harbor area

Seismic activity at the FFC site has been monitored with various instruments since August 2017 by both Advanced Seismic Instrumentation and Research (ASIR, 2021) and Uppsala University. A 4.5 Hz borehole geophone was installed at 620 m depth in the FFC-1 borehole in August 2017 and retrieved in February 2018 after indications of malfunction. A 2 Hz surface geophone was installed next to the FFC-1 borehole in October 2017 and in July 2018 a 4.5 Hz geophone was re-installed in the FFC-1 borehole, now at the bottom of the borehole, at approximately 2.1 km depth. The geophones operated until March 2020. Two broadband surface seismometers were installed in March 2018, one just outside the FFC facility and one at the Öresundsverken (ÖVT) district heating facility in Malmö harbor, 1.8 km away from FFC. These operated until May and April 2019, respectively. The FFC seismometer was re-installed in June–July 2020 for the drilling operations.

Prior to drilling, ASIR installed a 25 level, three-component, seismic array in the FFC-2 borehole in March 2020. The array had 75 m station spacing and extended to the bottom of the borehole at approximately 2.1 km MD. Additionally, two three-component geophones were installed by ASIR in the shallower boreholes FFC-3 (767 m) and ÖVT-1 (792 m).

The location of the FFC-1 borehole at a biofuel district heating plant in Malmö harbor, neighboring a metal recycling facility, a railroad, and a dock for shipping recycled metal (Fig. 3) implies a significant amount of human generated seismic noise. Impulsive, transient seismic events are present throughout the working day, but are less common during nights and weekends (Fig. 8a). There is also significant persistent noise at specific frequencies, originating, most likely, from pumps and fans in operation at the different facilities (Fig. 8b and c).

Fig. 8 shows that the transient noise signals can have amplitudes as high as 0.1 mm/s, and that persistent noise peaks have amplitudes of up to 100s of nanometer per second. These surface noise amplitudes are at such high levels that they make detection, location, and characterization of small earthquakes very difficult, especially during working hours. Recordings of daytime blasting in quarries located 20–25 km from FFC show that these events are not detectable at the surface at FFC, despite equivalent magnitudes of 1.0 to 1.2. Even the geophone at 2.1 km depth could not be used to detect these quarry blasts unless their existence and origin times were known. As a reference, the M 1.2 blast was clearly seen at a permanent Swedish National Seismic Network (SNSN) station 209 km away from the quarry. Due to the noise levels the seismic installations at FFC could therefore not be used to aid the national network in detecting earthquakes, although the deep sensor might provide data to enhance location accuracy.

These measurements of the background seismic environment are very valuable for the design of a seismic network that would be able to record microearthquakes during a geothermal stimulation. We found that in Malmö it will be necessary with several borehole installations, preferably below the 2.1 km thick sedimentary sequence.
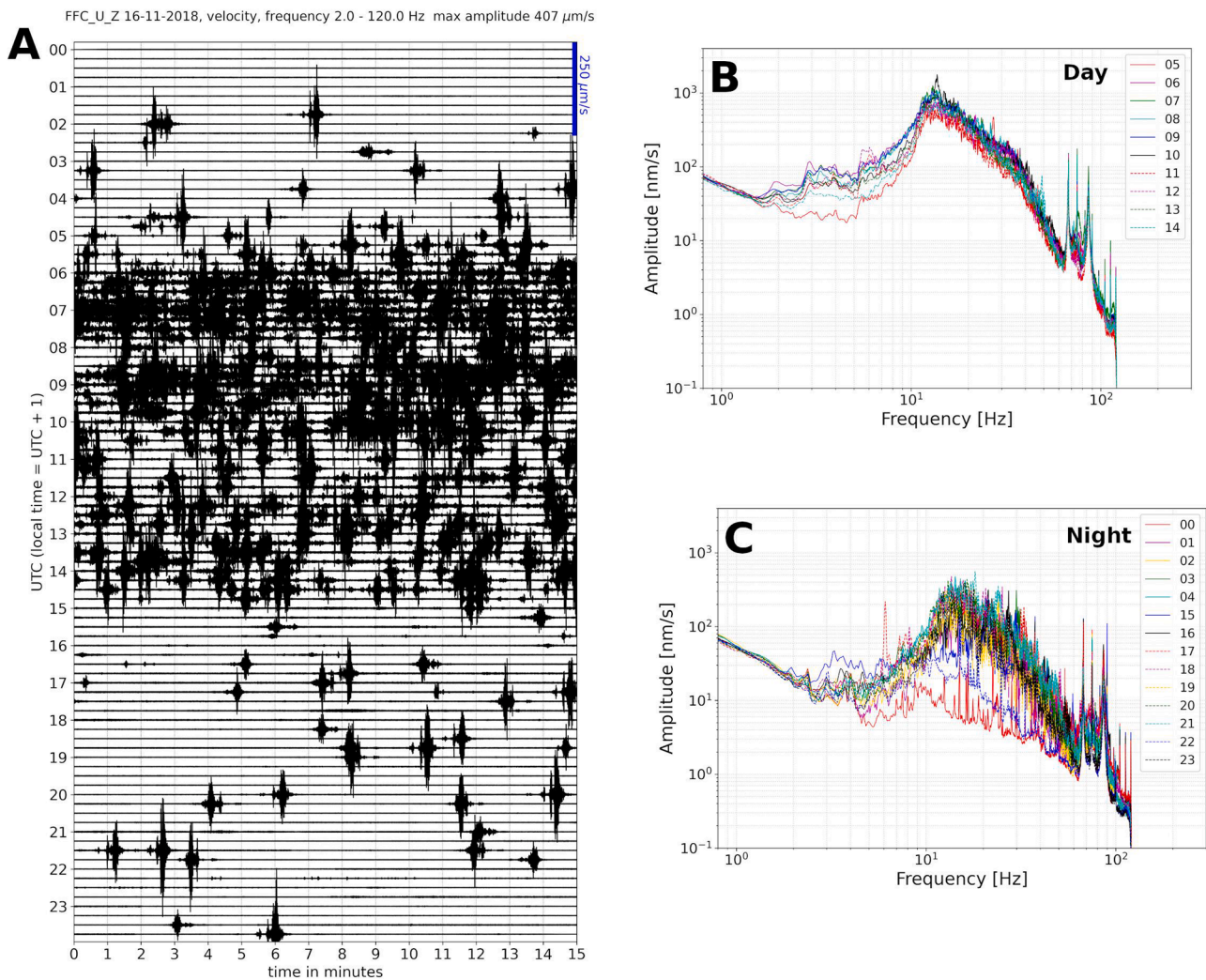
Fig. 8. a) Day plot of true ground motion seismic velocity data from the vertical component of the SNSN seismometer at FFC on 2018-11-16. Data are filtered between 2–120 Hz and displayed with 15 minutes of data per row. Times on the y-axis are in UTC, add one hour for Swedish times. The blue line in the upper right corner shows the amplitude scale of 250 μm/s. Maximum amplitude is noted in the title. b) Hourly spectra showing the spectral amplitudes of ground motion recorded by the SNSN seismometer at FFC on 2018-11-26 during working hours. c) Same as b) but during non-working hours.

3.4. Seismicity of southernmost Sweden

The seismic network operators in the Fennoscandian countries (Sweden, Norway, Denmark and Finland) all report recorded earthquakes to the FENCAT bulletin (FENCAT, 2021), maintained at the Institute of Seismology, Helsinki University. FENCAT also contains historical earthquake data back to the year 1375 (Ahjos and Uski, 1992). Fig. 9 shows earthquakes in southern Sweden and eastern Denmark from FENCAT up to 2006. From 2006 to 31 December 2019, we use the catalog of earthquakes detected by the SNSN (Lund et al., 2021). Unfortunately, there is only one permanent station in SNSN south of the STZ and the network is generally sparse in southern Sweden. In addition, the southwestern Sweden and Skåne stations were installed during 2006 – 2007, so there is only approximately 15 years of data from the region recorded by the modern SNSN. Only five earthquakes in the region have magnitudes larger than 4. Four of these occurred between 1985 and 2012, but only the 2008 event occurred on-land in Skåne. The magnitudes of the pre-2006 events are rather uncertain, as are their locations due to the very sparse station coverage and the instrument types. The SNSN has recorded three earthquakes within 15 km of central Malmö, and there are three more in the FENCAT data. We list these in Table 3. We do not include depths as there are no depth estimates for the older data and the estimates for the modern events are very uncertain due to

their location southwest of the seismic network. The lack of Rg waves for the three modern events indicate depths below 4–5 km, and the large M4.3 event in 2008 was located at 12–15 km depth.

Fig. 9 shows that many events in southernmost Sweden and in Kattegat are located along deformation zones and lineations associated with the STZ. There are very few events south of the STZ in Sweden. The 2008 M4.3 earthquake near Sjöbo occurred in the Vomb Trough of the STZ, north of the Romeleåsen Fault Zone, at approximately 12–15 km depth. Three M4+ events occurred in Kattegat at the northern boundary of the STZ, the 1985 and 2012 events on a fracture zone north of the STZ proper and the 1986 event on a deformation zone even further north in Kattegat. Two additional earthquakes with magnitudes larger than 3.5 have occurred in the active Kattegat region. The 1894 M3.7 event just east off the coast of Simrishamn also seems to have occurred in the STZ, possibly on its northern boundary, the seaward extension of the Kullen-Ringsjön-Andrarum Fault Zone, although the location likely has significant uncertainty associated with it. The 1930 M4.2 event south of the Falsterbo Peninsula is the only earthquake in the region with magnitude larger than 3.5 that is not associated with the core section of the STZ. It may have occurred on one of the NNW–SSE oriented fracture zones extending into the Baltic Sea from the Copenhagen area. The region has an unusually large number of M4+ events for Sweden and we note that the two largest events since the 1904 M5.4 Kosteröarna event on the
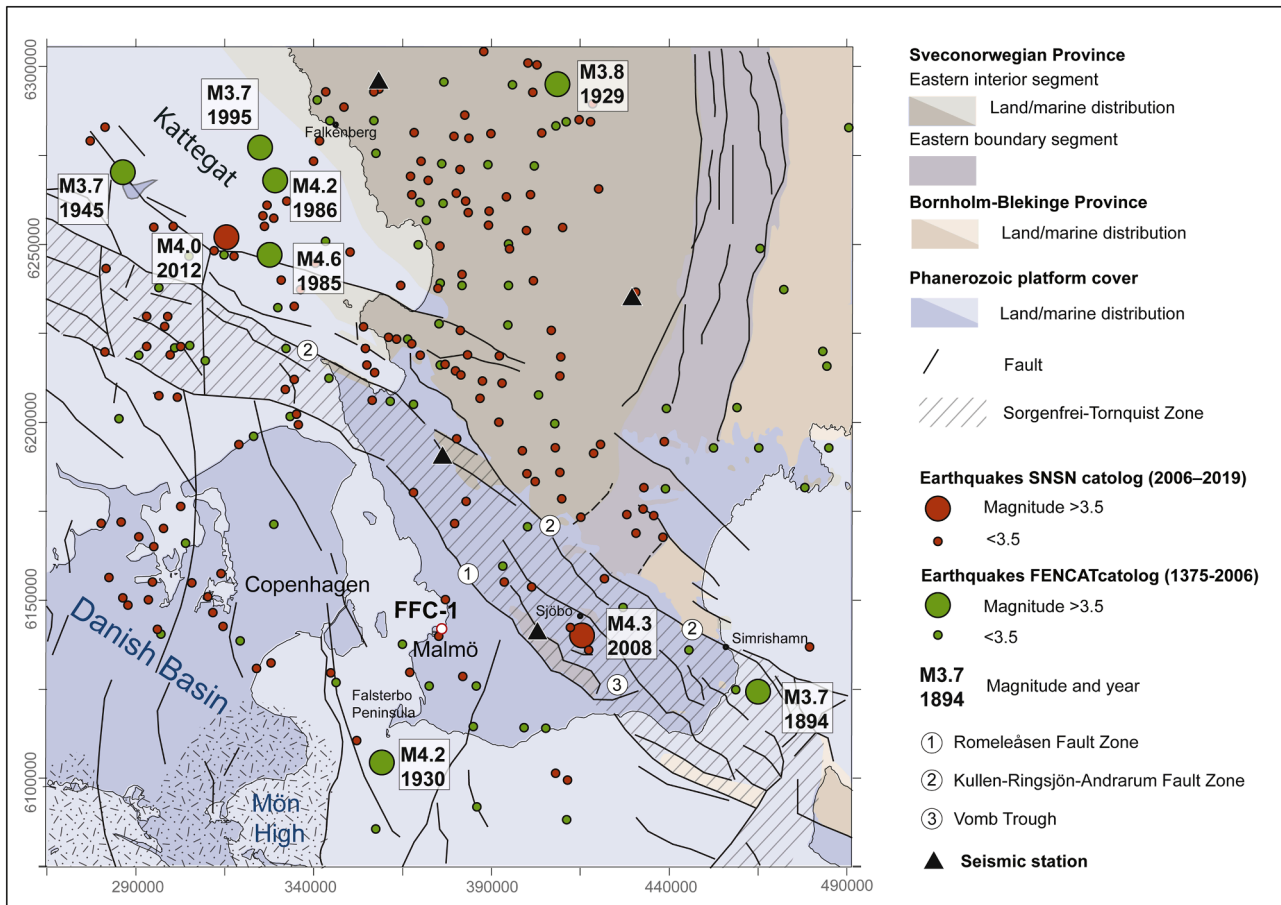
Fig. 9. Map of southern Sweden and eastern Denmark with earthquakes from the SNSN catalog (2006–2019) and FENCAT (1375–2006).

Table 3
Earthquakes recorded within 15 km of central Malmö. Events before 2000 come from FENCAT (FENCAT, 2021), events after 2000 from SNSN (SNSN, 1904).

Date	Time	Latitude	Longitude	Magnitude
1894-04-30	19:07	55.5	13.2	2.2
1914-07-22	01:30	55.5	13.0	2.2
1996-12-17	18:15	55.60	12.88	2.5
2011-05-03	17:49	55.624	13.035	0.1
2019-02-20	20:47	55.530	12.908	1.4
2019-05-02	23:56	55.524	13.134	1.1

west coast of Sweden (Bungum et al., 2009), the 1985 and the 2008 events, occurred here. There are no reports of damage from any of these two events. Interestingly, the 2008 M4.3 event was only followed by one, M0.3, aftershock in May 2009.

4. Interpretation

4.1. Source of reflectivity in the Precambrian

The sonic velocity in the crystalline part of the borehole generally lies in the 6.2–6.4 km/s range (Fig. 10), representing mainly the felsic gneiss. Two zones with velocities approaching, or exceeding, 7 km/s are present, one at about 2,300–2,335 m and another at about 3,025–3,130 m, the latter consisting of three units separated by thin gneiss sections. To compare the sonic log more directly to the seismic data a synthetic seismogram was generated. First the Vp and density logs were converted to time using the Vp log and setting the depth of 2,150 m equivalent to 1.3 s. Vp and density were then used to determine the reflectivity series

as a function of time. Finally, the reflectivity series was convolved with a 40 Hz Ricker wavelet with the result plotted on top of the surface seismic at the approximate subsurface location of the FFC-1 borehole (Fig. 10). In general, there is a good correlation between the synthetic seismogram and the surface seismic data, with the strongest responses coming at about 1.34 s (2,300 m) and at 1.575 s (3,020 m). The response at 1.34 s has higher amplitude than the later response due to the tuning effect of the mafic layer (maximum constructive interference occurs at a thickness of 40–45 m).

Aside from the correlation of the strongest reflections to mafic units there are some features in the seismic data to note. The relatively strong reflectivity above 1.34 s (2,300 m) may be related to increased fracturing observed from the base of sedimentary section to this depth. Effects of this fracturing may be seen in the sonic log (Fig. 10) at depths shallower than 2,300 m by the presence of several low velocity zones. An approximately 30 m thick low velocity zone is also present at 2,670–2,700 m, corresponding to about 1.45 s on the synthetic seismogram. This zone does not give a strong seismic response, probably due to that the top and bottom boundaries are gradational, rather than distinct as is the case with the amphibolites. A weak northward dipping reflection can perhaps be correlated to this zone. The thin amphibolite units between 2,335 m and 2,560 m all appear to correlate with weaker sub-horizontal reflections. It is reasonable to assume that most of the reflectivity observed from the Precambrian section in the western Malmö harbor profiles is generated by mafic lenses of amphibolite with varying thickness and lateral extent. These lenses appear to have a general sub-horizontal orientation. Finally, there appears to be a notable difference in the character of the reflectivity above 1.57 s (c. 3,000 m) and below. The interval from 1.35 s to 1.57 s is characterized by weak reflections with relatively high frequency whereas the response below
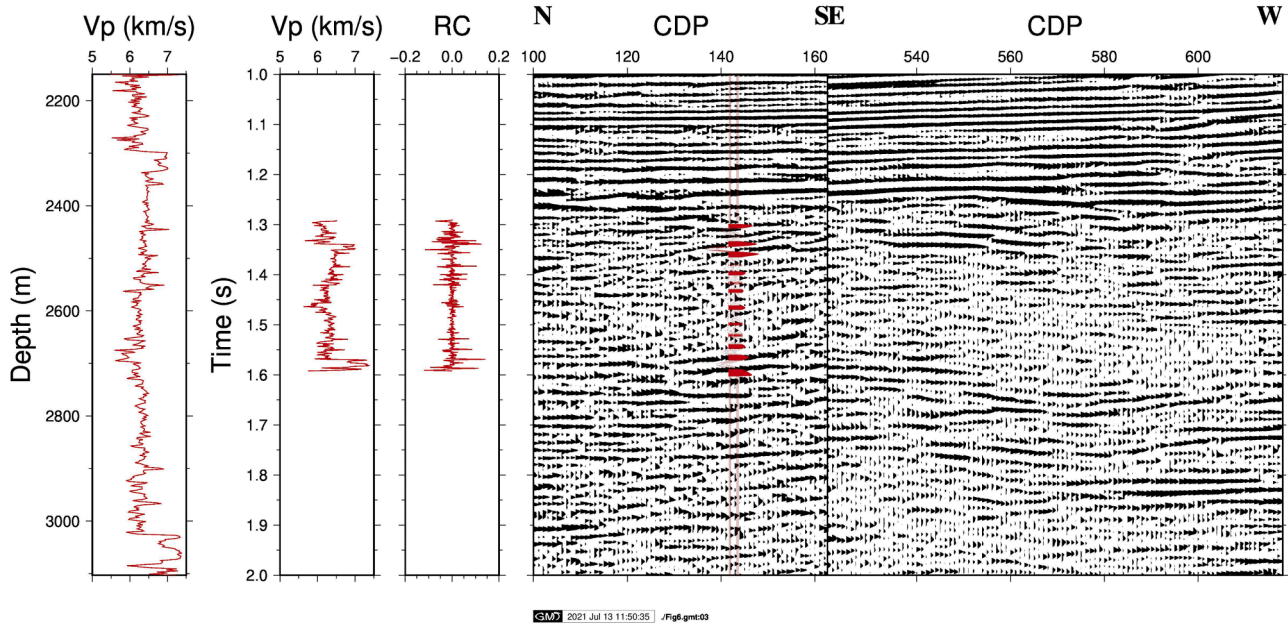
Fig. 10. (Panel 1) Velocity log after averaging and resampling to 1 m, (Panel 2) the velocity log converted to time and shifted 1.3 s, (Panel 3) reflectivity series calculated from velocity and density logs and (Panel 4) synthetic seismogram plotted on top of the surface seismic data. A 40 Hz Ricker wavelet was used to generate the synthetic seismogram.
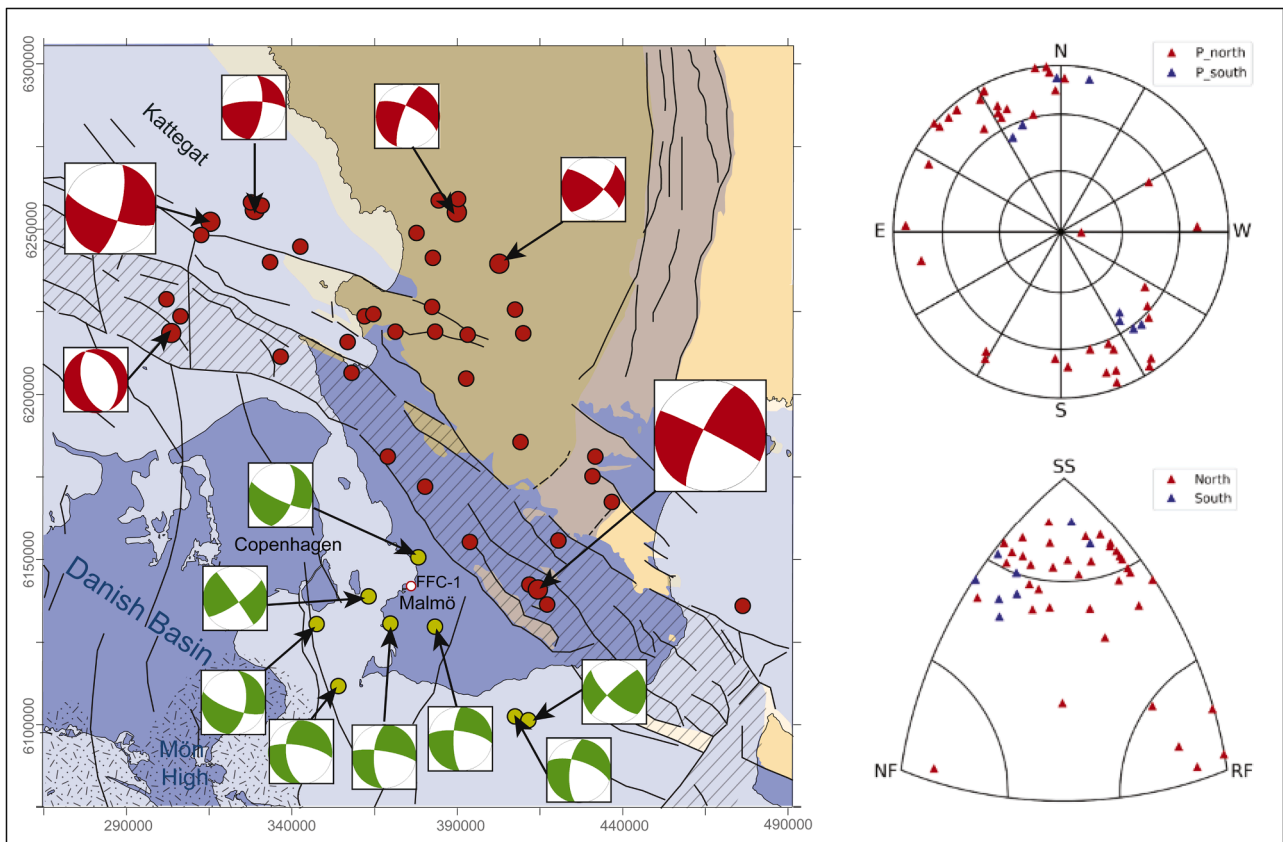

Fig. 11. Earthquakes used for stress inversion. Red circles and focal mechanisms are 40 events in, and north of, the STZ, mechanisms shown only for events with magnitude 3<M<4 (small), M>4 (large). Green circles and focal mechanisms are the eight events used for estimating stress in the south, all magnitudes. Legend to the geology is given in Figs. 2 and 9. Upper right: equal area projection of P-axes directions for the northern (red) and southern (blue) events. Lower right: Ternary plot (Kagan octant) of the faulting regimes, with strike-slip (SS) at the top, normal faulting (NF) at the bottom left and reverse faulting (RF) at the bottom right. Northern events are red, southern blue.

1.57 s is characterized by stronger more continuous reflections with lower frequencies. This may be due to an increase in the number and size of mafic lenses below 3,000 m. As mentioned earlier, there is no clear reflection from the top of the crystalline basement despite an expected large contrast in physical properties between the lowermost sedimentary units and the gneiss. This is probably due to the heavy fracturing in the uppermost crystalline basement reducing the velocity and density of the rock. The lack of a strong top of basement reflection can potentially be used as an indicator of heavy fracturing just below the sedimentary cover.

4.2. Stress field and fracture/fault stability

There is very little stress information available from Skåne. The World Stress Map (WSM), for example, contains a few single focal mechanisms and a few borehole data points for the region, none of which are south of the STZ. The WSM borehole data: hydraulic fracturing and overcoring measurements, come from two locations in the STZ and two locations north of the STZ and are all shallower than 200 m depth. The directions of the maximum horizontal stress vary from N37°E to N137°E, and from reverse to strike-slip conditions, in the boreholes in the STZ and from N17°E to N72°E, both reverse stress, in the boreholes north of the STZ. The large variations indicate that the measurements show local, near-surface stress states. In order to investigate the regional stress field around the STZ, and to obtain constraints on the stress field south of the STZ, we undertake an investigation of the recent earthquake focal mechanisms recorded by the SNSN. We divided the data into two sets, one northern with earthquakes in and north of the STZ, and one southern, south of the STZ (Fig. 11). For the northern set we select the southernmost 40 events which are recorded on at least six stations. As there are very few events recorded south of the STZ we use the eight events recorded at four or more stations. Focal mechanisms are calculated using both spectral amplitudes and polarities and generally have uncertainties of ±15°, which may be larger for the events recorded at only four stations, depending on the specific station coverage (Slunga, 1981; Rögnvaldsson and Slunga, 1993). Fig. 11 shows that most of the events have strike-slip mechanisms, with the northern events having one nodal plane being sub-vertical and striking NW–SE, in general

agreement with the STZ. These mechanisms suggest motion on planes aligned with the STZ and that there is a component of dextral deformation still occurring along the STZ, albeit at a very low level. There is one normal faulting event, the 2015 Kattegat event, and a few smaller reverse faulting events in the northern data set. The events south of the STZ have sub-vertical nodal planes that strike more N–S or E–W than the northern planes. The P-axes for both sets cluster around a general NNW–SSE direction (Fig. 11).

We invert the focal mechanisms of the two data sets for the causative state of stress (Lund and Slunga, 1999). The geometric information contained in the focal mechanisms imply that only the directions of the principal stress axes and a measure of the relative magnitude of the intermediate principal stress, $R = (S_1–S_2)/(S_1–S_3)$, can be recovered in the inversion. The results (Fig. 12a and b) are similar for the two data sets, with strike-slip states of stress and the maximum horizontal stress, SH (Lund and Townend, 2007), directed NNW–SSE. The northern set has the optimum SH directed N155°E with R=0.8 and the southern set N164°E, R=0.5. As seen in Fig. 12, the confidence intervals on the results of the southern set are relatively large, due to the very few events in the inversion, ranging from N–S to NW–SE within the 95% confidence interval.

Considering the strike of the STZ, which varies from approximately N110°E in the northwest to about N130°E in the southeast, the angle of the northern SH with respect to the fault zone direction is 25°–45°, indicating that it is close to optimally oriented for failure, assuming a coefficient of friction in the range 0.5–0.8 commonly found on faults. Reactivation of the STZ is thus not unexpected in the current stress field. Similarly, we can use the southern stress field to evaluate the relative stability of fractures in the FFC–1 borehole, under the assumption that the stress field at the site is the same. As the stress inversion does not provide the absolute magnitudes of the principal stresses we construct a synthetic stress state with one principal stress vertical, SH directed N164°E, R=0.5 and a coefficient of friction of 0.6 in order to obtain the maximum shear stress. Using Mohr-Coulomb theory we can then evaluate the relative stability of faults and fractures in this stress field. Fig. 12c shows the poles to the conductive fractures identified by CXD and SCMI logging of the FFC-1 well color coded by their relative stability in the southern stress field. The results indicate that the N–S striking
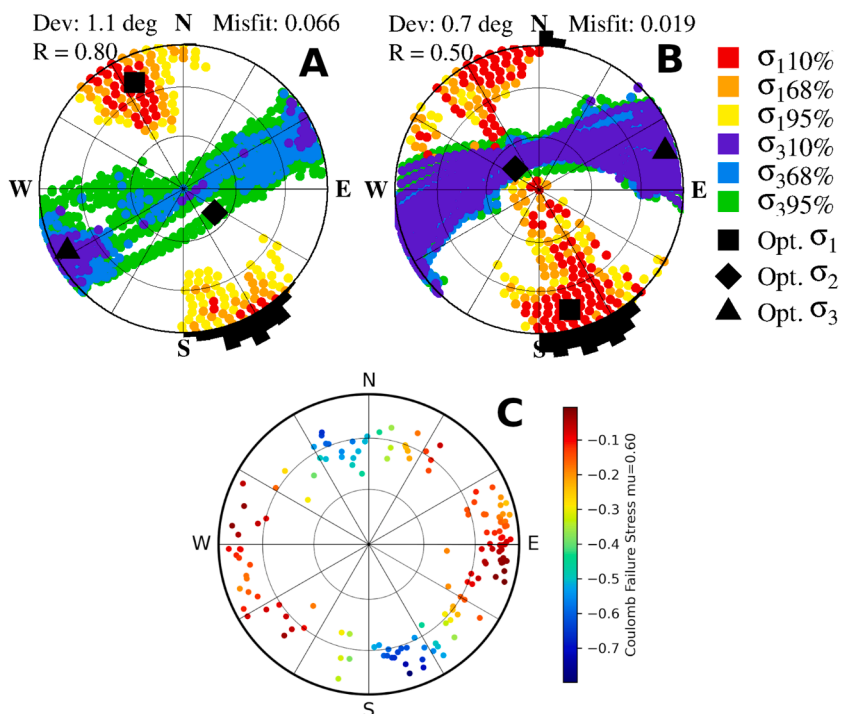

Fig. 12. Directions of the maximum and minimum principal stresses from inversion of focal mechanisms. a) The northern group, b) the southern group in Fig. 11. Lower hemisphere equal area projections, the black square shows the optimum direction of the maximum principal stress S₁ and the red to yellow circles are the 10%, 68% and 95% confidence regions. The black triangle shows the optimum direction of the minimum principal stress S₃ and the blue to green circles are the 10%, 68% and 95% confidence regions. The optimum direction of the intermediate principal stress S₂ is shown by a black diamond. The 95% confidence region of the maximum horizontal stress is indicated by the black histograms on the circumference of the plots. c) Relative stability of fractures identified in the FFC-1 borehole, evaluated with the stress state in b). Reddish colors are most unstable, bluish colors most stable.

fractures are most unstable in that stress field and that these fractures therefore would be most likely to conduct water (e.g. Barton et al., 1995). In addition, they are most easily stimulated in a geothermal stimulation operation, but are also most likely to slip, creating earthquakes, if the effective normal stress is significantly reduced.

5. Discussion

5.1. Coupling of results to the tectonic setting of southwestern Skåne

The general hypothesis of the main fracture orientation in SW Skåne is that it should follow the general alignment of the STZ, i.e., N110°E in the northwest to about N130°E to the southeast. Fracture data on outcrops inside the STZ in central Skåne also show a predominant fracture orientation following this trend (Müllern, 1978; Ising et al., 2019). In addition, fracture data just north of the STZ at Falkenberg give the same picture of a dominant NW–SE trend (Grigull and Andersson, 2019). Hence, the N–S dominant fracture orientation in FFC-1 surprisingly departs from this pattern, especially the ones assessed as conductive open in the image log. The NW–SE oriented fracture population, aligned with the STZ, is subordinate in the FFC-1 well. To some extent the N–S fracture orientation in FFC-1 is supported by a N–S oriented population of fractures in the Danian limestone in a quarry at Limhamn, a few kilometers south of the FFC-1 drill site. These have been interpreted as due to relatively recent N–S far-field compression in the area, probably related to Iberian plate collision with south Europe, i.e. the Pyrenean phase (Bergerat et al., 2007). This observation shows the presence of a N–S oriented population, which is likely also portrayed in the upper part of the crystalline basement, but it does not clarify the puzzling significant absence of a fracture population in FFC-1 like what we see dominate inside the STZ.

The divergent fracture orientations between FFC-1 and STZ could originate from the fact that the crystalline bedrock in Skåne displays a complex mixture of fracturing and faulting from brittle phases of deformation during the Caledonian, Variscan and Alpine orogens. Several different principal stress regimes prevailed in Skåne during these events, including mainly NE–SW and NW–SE extensions, and NE–SW compression (Erlström et al., 1997; Bergerat et al., 2007; Erlström, 2020). The tectonic signature also reflects repeated phases of dextral strike-slip with releasing and restraining bends, which have in combination with both extension and compression led to locally varying prerequisites for the orientation and magnitude of the local stress field as well as the fracturing. Sivhed (1991), Blundell et al. (1992), Thomas and Deeks (1994), Thybo (1997), Mogensen (1994, 1995) and Erlström and Sivhed (2001) have all described how strike-slip movements were a significant component in the tectonic regime during both extension and compression phases centred around the Sorgenfrei-Tornquist Zone. Push-up compression and relaxation structures associated with releasing or restraining conditions are found both in the Kattegat area (Mogensen, 1994; 1995), along the Romeleåsen Fault Zone at Dalby and the Fyledalen Fault Zone in central Skåne (Erlström et al., 2004) as well as in the Bornholm Gat proper (Deeks and Thomas, 1995). Thus, this inherited tectonic signature and structural framework may still be portrayed in the local fracture setting.

There is also the influence from an NNW–SSE oriented Triassic normal fault, indicated in the vicinity of FFC-1 on the seismic lines MVL01/05 and MVL02/07 to consider. The fault is interpreted to be derived from NW–SE oriented Triassic extension and coupled to a suite of NNW–SSE and N–S oriented normal faults encompassing the Höllviken Graben i.e., the Öresund, Amager and Svedala faults (Erlström et al., 2018; Erlström, 2020). The fault throw is small and not resolved in the seismic data. The fault is interpreted to dip c. 70° to the west and seen as a zone of disrupted and terminating reflections in the crystalline basement just below the FFC-1 well. In addition, there are also offshore, to the north and south of FFC-1 a few minor NW–SE and NNW–SSE striking faults younger than Triassic indicated in the

sedimentary succession. These affected mainly the pre-Cretaceous, but minor Late Cretaceous and Paleogene reactivation is seen as small-scale disturbances in the seismic profiles.

Although there is significant uncertainty in both the stress determination from the focal mechanisms (only eight earthquakes) and borehole stress indicators, the data sets suggest that there is a more N–S direction of the maximum horizontal stress in FFC-1 than in southwestern Skåne in general. The few borehole stress indicators are restricted to a limited depth interval, implying that the differential stress is low compared to the rock strength. Such a N–S orientation of SHmax is consistent with the N–S fractures being electrically conductive, and open. We do note, however, that the earthquake derived stress field would imply hydrologically conductive fractures in the N–S direction, further complicating the inferences on the FFC-1 stress field. A comprehensive stress measurement campaign is necessary to resolve the stresses in FFC-1.

A N–S oriented SHmax could be explained either by local perturbations caused by the presence of local faults, such as the Triassic fault close to FFC-1 discussed above which has seen later movement, or by a reorientation of the stress-field related to variations of the thickness and rigidity of the lithosphere between the STZ, the Fennoscandian Shield and younger geological provinces to the south. Most of the focal mechanism data south of STZ show a P-axis direction that is consistent with the NW–SE trend found north of the STZ. However, there is one focal mechanism just west of the FFC-1 site that may indicate a deviation of the stress field towards a more northerly direction (cf. Fig. 11). A potential source of difference in the stress estimates is that the observed focal mechanisms are below 5 km depth in the crystalline basement and that the stresses could be perturbed and deviating at shallower depth in the upper part of the crystalline crust, as well as in the overlying sedimentary succession. Note that there are no stress measurements in the about 2.1 km thick sedimentary succession in FFC-1.

Beside the focal mechanisms from earthquakes presented in this paper no other indicators of the current orientation of the stress field exists in SW Skåne. World Stress Map data from north Germany based on break-out data in wells (Heidbach et al., 2018) and recent modeling show that a contemporary N–S orientation of the maximum horizontal stress prevails in northern Germany, and likely also in the southern part of the Danish Basin (Ahlers et al., 2021). Again, these data are only from the sedimentary succession.

5.2. Comparison with other seismic data

Outside of mineral exploration areas, relatively few deep boreholes have been drilled into the crystalline crust where surface seismic data are available despite hundreds of thousands of kilometers of seismic profile having been acquired. Two notable examples in Sweden, aside from the present study, where coincident borehole and surface seismic data are available are the Siljan Ring area and the Jämtland area (Fig. 2). In the Siljan Ring area (Juhlin, 1990) several distinct, mainly continuous, sub-horizontal, high amplitude reflections are observed in the upper 10 km of crust. Drilling into these revealed that mafic dolerites in granitic bedrock are generating the strong reflections. Image logs at Siljan also showed pervasive borehole breakouts and occasional drilling induced fractures from 2 to 6.5 km depth (Lund and Zoback, 1999). This is a rather different setting than is the case in the Malmö harbor area. In the Jämtland area a project has been ongoing since about 2010 (Gee et al., 2010) to better understand the structure of the Swedish mountain belt through the Collisional Orogeny in the Scandinavian Caledonides (COSC) project. The first borehole (COSC-1; Lorenz et al., 2015) was drilled into the highly reflective Seve Nappe and penetrated mainly felsic gneiss with minor amphibolite to about 2.5 km depth (Hedin et al., 2016). Analysis of log data, core and the surface seismic data from the area show that it is highly likely that it is lenses of amphibolite in a gneiss matrix which are generating the reflections. The lateral extension of the reflections and their amplitude are dependent upon the size of the lenses. This is a situation like what we interpret to be present in the

Precambrian rock in the Malmö harbor area. For comparison the seismic data over the COSC-1 borehole corresponding to the Seve Nappe are plotted on the same scale as the reflective Precambrian section along the western part of the MVL01/05 profile in Fig. 13. The two seismic sections show a similar character, supporting the suggestion that the lithologies generating the reflectivity at the two different sites have some similarities to one another.

5.3. Relevance for geothermal exploration in crystalline rock

The temperature data acquired in FFC-1 is a valuable contribution to understanding temperature variations in the Fennoscandian basement. So far, there are only a few deep wells (>2 km) in the Fennoscandian basement where temperature measurements have been conducted. The temperature measurements in FFC-1 were acquired about three months after the drilling was stopped and at temperature conditions different than the pre-drilling conditions. However, the measured temperatures still give an indication of the general temperature conditions in the well. The bottom hole temperature of 84.1°C in FFC-1 is 10°C higher than the temperature measured at the same depth in the DGE-1 well. The wells are located approximately 20 km apart. The calculated temperature gradient, 2.35°C/100 m in the upper part of the crystalline basement, down to 2,610 m MD, in FFC-1 is 1.5°C/100 m higher than that calculated for the crystalline basement part of DGE-1. The gradient is also higher than the ones measured in other deep wells located in the Fennoscandian Shield, such as Gravberg-1, OTN-1–3, Outokumpu R-2500, where gradients between 1.4 and 1.8°C/100 m are reported (Juhlin et al., 1998; Kukkonen et al., 2011; Kukkonen and Pentti, 2021). In FFC-1 a lower gradient, 1.74°C/100 m, is found below 2,880 m depth, which is more like the gradients reported for the previously mentioned wells. A more detailed evaluation of the temperature data acquired in FFC-1 and a comparison with temperature data from other wells are presented in Rosberg and Erlström (2021).

The reflection seismic data from the Malmö harbor area are of surprisingly good quality given the high noise levels of the urban environment that they were recorded in. Since most suitable locations for deep geothermal projects in the Fennoscandian Shield will be at urban locations the success of obtaining good images at Malmö can serve as a guide for planning reflection seismic surveys at other sites. Seismic data primarily provide structural information that can be related to geology. They do not generally provide direct detection of fractured rock. Experience has shown that most reflectivity observed on seismic surveys over crystalline rock can be attributed to lithological boundaries although there are important exceptions. For the Malmö case they show that the crust is heterogeneous below the sedimentary cover and that the gently dipping discontinuous reflections are primarily generated by density anomalies related to the occurrence of mafic amphibolite bodies and lenses in the felsic gneissic host rock. Potential steeply dipping fracture zones can be inferred by offsets in the sub-horizontal reflectivity or by near-vertical transparent zones, but any such interpretations should be treated with caution. The lack of a clear top of basement reflection is judged to indicate that the uppermost crystalline basement is highly fractured at FFC. This point was not stressed in the pre-drilling stage. However, if it had been then this could have guided the choice of drilling technology and potentially saved significant costs to the project. High quality seismic data have the potential to allow better planning of where to drill and, perhaps, how to drill and should be considered an asset to deep geothermal projects. They also allow a better understanding of the geology around the borehole to be gained than only cuttings or logging data provide since features can be extrapolated away from the borehole.

The characteristics of the fracture framework regarding frequency, distribution, orientation, and openness is of great importance in assessing the potential for an enhanced geothermal system in the crystalline basement. As described in Rosberg and Erlström (2021), the fracture frequency and fracture volumetric density were found to be relatively high in comparison to the limited number of similar observations at other locations in crystalline rock. It was also noted from the SCMI data that between 2,450 m and 2,700 m the fractures were evenly distributed with a relatively high linear fracture frequency. Below 2,700 m the fractures are commonly occurring in clusters and the linear fracture frequency is also slightly lower than above. Note that above 2,450 m there were gaps in the SCMI-data due to the poor hole conditions.
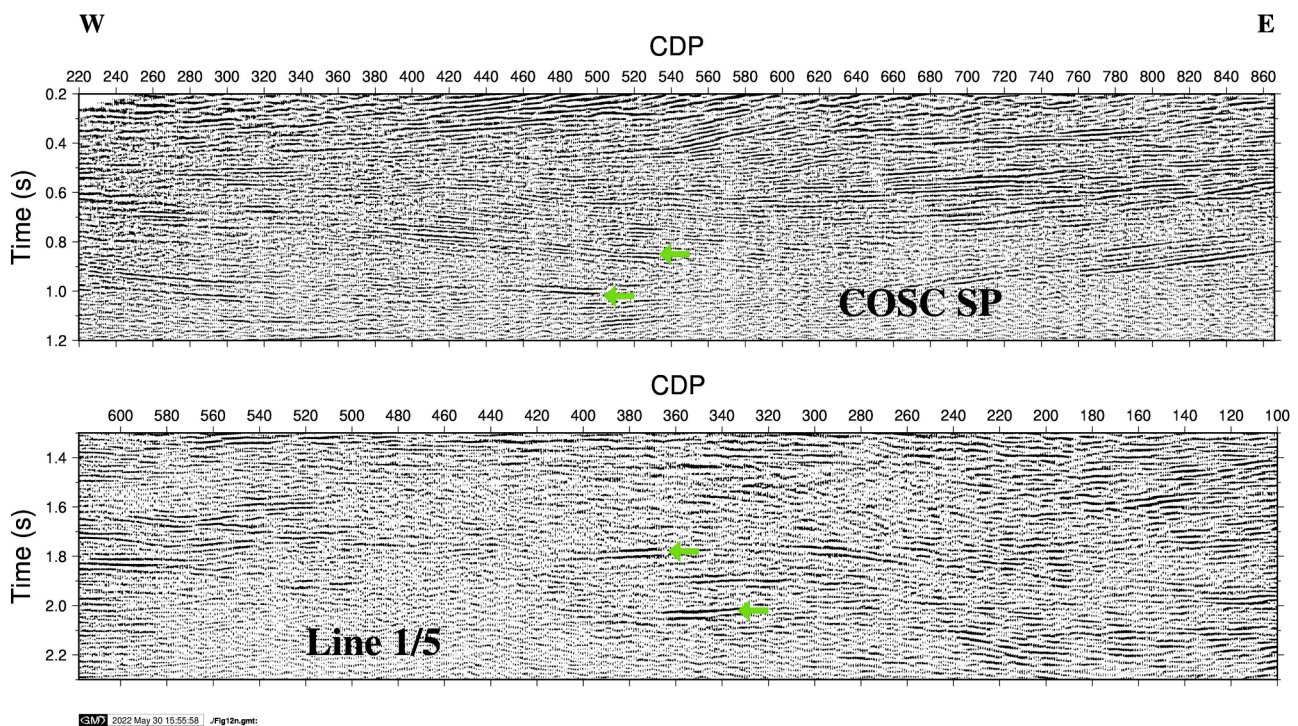

Fig. 13. Seismic section over the Seve nappe in western Jämtland, Sweden (top) plotted at the same scale as the Skåne data (bottom). Green arrows indicate examples of reflections that may be generated by mafic lenses.

Limited locations are available for comparison of the fracture data in FFC-1, making it difficult to evaluate FFC-1 data with respect to the ability to hydraulically stimulate the crystalline basement by enhancing the existing fracture network for a deep geothermal reservoir. A few comparable values on the linear fracture intensity for the Fennoscandian crystalline basement are described from much shallower boreholes in granitoid rocks at Laxemar, on the east coast of Sweden. These give for one-kilometre-deep boreholes, an open fracture frequency usually below 3 frac/m and a volumetric fracture density of 1.4–4.6 m^2/m^3 (La Pointe et al., 2008; SKB, 2009). Thus, not very different from the values obtained in the FFC-1 well, but for considerably shallower depth. Outside the Fennoscandian Shield the deep geothermal projects in Basel in Switzerland, Soultz-sous-Forêts in France and the Rosemanowes site in the UK give fracture spatial distribution signatures normally below one fracture per meter for the basement between 2,000 to 5,000 m (Meet, 2019). In the United Downs geothermal project in Cornwall (UK) fracture frequencies of 2.1, 1.6, 1.2 and 0.3 frac/m were observed for four granite-dominated intervals between c. 1 and 5 km depth, where the two higher values were noted above 4 km (Reinecker et al., 2021). In the KTB deep borehole in Germany a corresponding fracture frequency of less than 0.3 fractures per meter is reported between 6,900 and 7,135 m depth (Zimmermann et al., 2000). Although considerably deeper, a significantly lower value than in FFC-1.

The rock mass strength and ability to activate the fractures by hydro-shearing depends not only on the fracture frequency, but also on the relative amounts of open fractures and the volumetric fracture density. Open fractures constitute a relatively large part of the fractures in FFC-1, especially in the relatively highly fractured interval between 2,562 and 2,695 m. A semi-quantitative estimation using the excess conductivity method after Luthi and Souhaité (1990) gives an average fracture aperture of 0.422 mm with values of up to 7–12 mm in the 2,562–2,695 m interval. Moreover, data from tunnelling in crystalline rocks at considerably shallower depth indicate for instance that a transition from a massive to kinematically controlled blocky rock mass takes place when the volumetric fracture density rises above 2–2.5 m^2/m^3 (Rogers et al., 2015).

When assessing and comparing the FFC-1 fracture data, the interval between 2,562 and 2,695 m with a fracture frequency (2.49 frac/m), volumetric fracture density (3.39 m^2/m^3) and high spatial distribution of open and hydraulically active fractures stands out as a potentially kinematically active rock mass that could be stimulated as an EGS reservoir. The fracture frequency is calculated on all fractures that are interpreted as fully or partially conductive, thus, assumed to be potentially feasible to be enhanced by hydraulic stimulation.

However, the temperature is insufficient (77–80°C) for direct heat exchange to the district heating system in Malmö. Localizing comparable fractured intervals, as the 2,562–2,695 m interval, at appropriate temperature-depths of 5–6 km (i.e. >120°C) is judged to be the most plausible way forward for an EGS in the crystalline basement beneath Malmö. The less favourable thermal conductivity of the amphibolite also points to that the gneiss intervals with significantly higher thermal conductivity have the best prerequisites for creating a deep EGS reservoir in Malmö. The ratio between these two dominating rock types plays naturally a significant role for the thermal property of the rock mass. However, changes in thermal conductivity could be levelled out by convection provided that the fracture networks are much the same and that the amphibolite/metabasite occur as isolated minor lenses in the gneiss. The above discussion demonstrates the importance of characterizing the rock mass using seismic methods prior to drilling in order to optimize target depth and borehole locations.

Data on earthquakes in the region where a geothermal power plant is planned is crucial both to estimate the earthquake hazard and to provide data for a regional stress estimate. The current SNSN can detect and locate earthquakes down to approximately magnitude 0.5 within the network (Lund et al., 2021), but has only been in operation at this level for 15–20 years, depending on the region. Complementing the SNSN

data with the installation of a few seismic stations at the intended geothermal site, preferably one to two years prior to stimulation, will provide further data on small local earthquakes and therefore improve the hazard assessment. In addition, the local data will give information on the seismic noise environment and thus aid the design of the local seismic network which will be needed both during the stimulation phase and the later operation of the geothermal power plant.

The regional stress field obtained from earthquake focal mechanisms can readily be used with regional and local fault data to assess the reactivation potential of larger geological structures, which will improve the seismic hazard assessment. The stress data can also be used with logging data on fracture orientations to assess which fracture orientations are most likely to conduct water, or to be most amenable for stimulation. It will also give an indication of which fracture orientations are most likely to fail in earthquakes. However, it is important to note that the regional stress field is based on earthquakes generally occurring at 10–15 km depth, significantly deeper than the boreholes that would be used for heat extraction. The earthquake derived stress field is also a regional average which may not be representative for the site unless that are many events in the vicinity. Therefore, it is important to carry out dedicated stress measurements in a borehole at the site, preferably to the depths where stimulation is intended. In-situ stress field determinations will provide both directions and magnitudes of the principal stresses and thus give a better indication of the local fracture conductivity and stability, and provide important data both for geothermal reservoir modeling and seismic hazard assessment.

6. Conclusions

Deepening of the FFC-1 well to 3,133 m measured depth into the uppermost kilometer of the Precambrian basement has provided significant additional data that can be used to evaluate the potential of EGSs in southern Sweden. Combined with the existing reflection seismic data a better understanding of the lithology and structure in the uppermost crust has been obtained. Gently dipping lenses of mafic amphibolite embedded in a gneissic matrix generate most of the observed reflectivity. Fracturing is relatively high in the drilled interval with heavy fracturing in the interval extending from just below the sedimentary succession (c. 2.1 km) down to about 2.3 km MD. This heavy fracturing, resulting in reduced seismic velocities, may explain the lack of a clear reflection off the top of the crystalline basement. Below 2.3 km fracturing is still relatively high in comparison to other locations, with open and induced fractures having mainly a N–S orientation. This orientation is inconsistent with that expected from the regional stress field based on seismicity studies in the area with a maximum horizontal stress in the NW–SE direction. There are no breakouts in the borehole and only a handful of short drilling induced tensile fractures, indicating a N-S direction of the maximum horizontal stress and that the differential stress is generally lower than the rock strength. The local stress field may differ from the regional stress field in southwestern Skåne due to depth variations, the earthquakes are located deeper than the borehole, or to potential steeply dipping faults zones in the area near the well. Still, the unexpected N–S orientation give an unique insight to that the stress situation on the margins of the Fennoscandian Shield is more complex than anticipated, especially on the local scale. It also demonstrates the importance of in-situ measurements of the stress field to understand the expected response of the rock mass to stimulation. Temperatures of around 80°C at 3 km suggest that 120°C may be reached already at 5 km depth. If the degree of fracturing is as high at 5 km as in the interval drilled below 2.3 km then the potential for heat extraction exists if drilling can be done economically and stimulation controlled.

CRediT authorship contribution statement

Christopher Juhlin: Conceptualization, Methodology,

Investigation, Writing – review & editing. **Mikael Erlström:** Methodology, Investigation, Writing – review & editing, Funding acquisition. **Björn Lund:** Methodology, Investigation, Writing – review & editing, Funding acquisition. **Jan-Erik Rosberg:** Methodology, Investigation, Writing – review & editing, Funding acquisition.

Declaration of Competing Interest

The authors declare that they have no known competing financial interests or personal relationships that could have appeared to influence the work reported in this paper.

Acknowledgments

References

Ahjos, T., Uski, M., 1992. Earthquakes in northern Europe in 1375-1989. Tectonophysics 207, 1–23.

Ahlers, S., Henk, A., Hergert, T., Reiter, K., Muller, B., Röckel, L., Heidbach, O., Morawietz, S., Schenck-Wenderoth, M., Anikiev, D., 2021. 3D crustal stress of Germany according to a data-calibrated geomechanical model. Solid Earth 12, 1777–1799. https://doi.org/10.5194/se-12-1777–2021. Doi-org/.

ASIR, 2021, https://asirseismic.com/, last visited 2021-06-22.

Balling, N., 1990. Heat flow and lithospheric temperature along the northern segment of the European Geotraverse. In: Freeman, R., Mueller, St. (Eds.), Proceedings of the 6th Workshop of the European Geotraverse (EGT) Project. European Science Foundation, Strasbourg, pp. 405–416.

Balling, N., 1995. Heat flow and thermal structure of the lithosphere across the Baltic Shield and northern Tornquist Zone. Tectonophysics 244, 13–50.

Barton, C.A., Zoback, M.D., Moos, D., 1995. Fluid flow along potentially active faults in crystalline rock. Geology 23, 683–686.

Bergerat, F., Angelier, J., Andreasson, P-G., 2007. Evolution of paleostress fields and deformation of the Tornquist Zone in Scania (Sweden) during Permo–Mesozoic and Cenozoic times. Tectonophysics 444, 93–110.

Bjelm, L., Alm, P.-G., 2010. Reservoir cooling after 25 years of heat production in the Lund geothermal heat pump project. In: Proceedings World Geothermal Congress. Bali, Indonesia. April 25–29, 2010.

Bjelm, L., Persson, P.-G., 1981. Geotermisk energiutvinning i Skåne Slutrapport Etapp 4 (in Swedish), TVGL-3013. Department of Engineering Geology, Lund University report, LUTVDG, pp. 1–52.

Bjelm, L., Hartlèn, J., Röshoff, K., Bennet, J., Bruch, H., Persson, P.-G., Wadstein, P., 1977. Geotermisk energiutvinning i Skåne Slutrapport Etapp 1(in Swedish), TVGL-5013. Department of Engineering Geology, Lund University report, LUTVDG, pp. 1–50.

Bjelm, L., Hartlèn, J., Röshoff, K., Bennet, J., Bruch, H., Persson, P.-G., 1979. Geotermisk energiutvinning i Skåne Slutrapport Etapp 2 och 3 (in Swedish), TVGL-3003. Department of Engineering Geology, Lund University report, LUTVDG, pp. 1–95.

Blundell, D., Freeman, R., Mueller, S., 1992. A Continent Revealed. The European Geotraverse. Cambridge University Press, Cambridge, pp. 1–261.

Bungum, H., Pettenati, F., Schweitzer, J., Sirovich, L., Faleide, J.I., 2009. The 23 October 1904 M_S 5.4 Oslofjord earthquake: reanalysis based on macroseismic and instrumental data. Bull. Seismol. Soc. Am. 99, 2836–2854. https://doi.org/10.1785/0120080357.

Ciuperca, C.-L., Camil, B., Erlström, M., Hammar, A, Egard, M., 2021. An integrated formation evaluation approach evaluated the basement temperature anomaly. In: EAGE 82nd Conference and Exhibition, Amsterdam, extended abstract, p. 4.

Deeks, N., Thomas, S.A., 1995. Basin inversion in a strike-slip regime: the Tornquist Zone, Southern Baltic Sea. Geol. Soc. Spec. Publ. 88 (1), 319–338. https://doi.org/10.1144/GSL.SP.1995.088.01.18.

Eriksson, K.-G., Ahlbom, K., Landström, O., Larson, S.-Å., Lind, G., Malmqvist, D., 1978. investigation for geothermal energy in Sweden. Pure Appl. Geophys. 117, 196–204.

Erlström, M., Sivhed, U., 2001. Intra-cratonal dextral transtension and inversion of the southern Kattegat on the on the southwest margin of Baltica – seismostratigraphy and structural development. Geol. Surv. Sweden C 832, 1–33.

Erlström, M., Deeks, N., Sivhed, U., Thomas, S., 1997. Structure and evolution of the Tornquist Zone and adjacent sedimentary basins in Scania and the southern Baltic Sea area. Tectonophysics 271, 191–215.

Erlström, M., Sivhed, U., Wikman, H., 2004. Beskrivning till berggrundskartorna 2D Tomelilla NV, NO, SV, SO 2E Simrishamn NV, SV 1D Ystad NV, NO 1E Örnahusen NV. Sveriges geologiska undersökning ser Af 211–214, p. 141.

Erlström, M., Boldreel, L.O., Lindström, S., Kristensen, L., Mathiesen, A., Andersen, M.S., Nielsen, L.H., 2018. Stratigraphy and geothermal assessment of Mesozoic sandstone reservoirs in the Øresund Basin – exemplified by well data and seismic profiles. Bull. Geol. Soc. Den. 66, 123–149.

Erlström, M., 2020. Chapter 24: carboniferous–neogene tectonic evolution of the Fennoscandian transition zone, southern Sweden. In: Stephens, M.-B., Bergman Weihed, J. (Eds.), Sweden Lithotectonic Framework, Tectonic Evolution and Mineral Resources, Sweden Lithotectonic Framework, Tectonic Evolution and Mineral Resources, 50. Geological Society Memoir, pp. 603–620.

EUGENO-s Working Group, 1988. Crustal structure and tectonic evolution of the transition between the Baltic Shield and the North German Caledonides. Tectonophysics 150, 253–348.

FENCAT, 2021. https://www.helsinki.fi/en/institute-of-seismology/bulletins, visited on 2021-06-21.

Gee, D.G., Juhlin, C., Pascal, C., Robinson, P., 2010. Collisional orogeny in the Scandinavian caledonides. GFF 132, 29–44.

Gehlin, S., Andersson, O., Rosberg, J.-E., 2020. Country update for Sweden 2020. In: Proceedings World Geothermal Congress 2020 Reykjavik. Iceland, p. 9. April 26 – May 2.

Grigull, S. and Andersson, J., 2019. Brittle structures at the Stavsjö quarry, Falkenberg. Geological survey of Sweden report 2019:05, 18 pp.

Hedin, P., Almqvist, B., Berthet, T., Juhlin, C., Buske, S., Simon, H., Giese, R., Krauß, F., Rosberg, J.-E., Alm, P.-G., 2016. 3D reflection seismic imaging at the 2.5 km deep COSC-1 scientific borehole, central Scandinavian caledonides. Tectonophysics 689, 40–55.

Heidbach, O., Rajabi, M., Cui, X., Fuchs, K., Müller, B., Reinecker, J., Reiter, K., Tingay, M., Wenzel, F., Xie, F., Ziegler, M., Zoback, M.-L., Zoback, M., 2018. The world stress map database release 2016: crustal stress pattern across scales. Tectonophysics 744, 484–498. https://doi.org/10.1016/j.tecto.2018.07.007.

Henkel, H., Bäckström, A., Bergman, B., Stephansson, O. and Lindström, M., 2005. Geothermal energy from impact craters? The Björkö study, Proceedings, World Geothermal Congress 2005, Turkey, 5 pp.

Ising, J., Bergström, U., Erlström, M., Grigull, S., Malmberg-Persson, K., Wickström, L., Lundquist, L. and Engdahl, M., 2019. Hässleholm-Lund – uppgraderad geologisk information inför projektering av höghastighetsjärnväg. Sveriges geologiska undersökning rapport 2019:03, 52 pp. [in Swedish].

Juhlin, C., Wallroth, T., Smellie, J., Leijon, B., Eliasson, T., Ljunggren, C., Beswick, J., 1998. The Very Deep Hole Concept - Geoscientific Appraisal of Conditions at Great Depth, p. 128. Swedish Nuclear Waste Programme Technical Report SKB-TR-98-05.

Juhlin, C., 1990. Interpretation of reflections in the Siljan Ring area based on results from the Gravberg-1 borehole. Tectonophysics 173, 345–360.

Klitzsch, N., Ahrensmeier, C., 2021. Thermal Matrix Properties Measured on Cuttings from the Malmö Well. Aachen University, p. 7 report.

Kukkonen, I.T., Pentti, M., 2021a. St1 deep heat project: geothermal energy to the district heating network in Espoo. IOP Conf. Earth Environ. Sci. 703, 012035.

Kukkonen, I.T., Rath, V., Kivekäs, L., Šafanda, J., Cermak, V., 2011. Geothermal studies of the Outokumpu deep drill hole, Finland: vertical variation in heat flow and paleoclimatic implications. Phys. Earth Planet. Inter. 188, 9–25.

La Pointe, P., Fox, A., Hermanson, J., Öhman, J., 2008. Geological Discrete Fracture Network Model for the Laxemar Site -Site Descriptive Modelling SDM-Site Laxemar, p. 260. SKB report R-08-55.

Libouriussen, J, Ashton, P., Tygesen, T., 1987. The tectonic evolution of the Fennoscandian border zone. Tectonophysics 137, 21–29.

Lorenz, H., Rosberg, J-E., Juhlin, C., Bjelm, L., Almqvist, B., Berthet, T., Conze, T., Gee, D., Klonowska, I., Pascal, C., Pedersen, K., Roberts, N., Tsang, C-F., 2015. COSC-1-drilling of a subduction-related allochthon in the Palaeozoic Caledonide orogen of Scandinavia. Sci. Drill. 19, 1–11.

Lund, B., Slunga, R., 1999. Stress tensor inversion using detailed microearthquake information and stability constraints: application to Ölfus in southwest Iceland. J. Geophys. Res. 104 (14), 964, 947-14.

Lund, B., Townend, J., 2007. Calculating horizontal stress orientations with full or partial knowledge of the tectonic stress tensor. Geophys. J. Int. 170, 1328–1335. https://doi.org/10.1111/j.1365-246X.2007.03468.x.

Lund, B., Zoback, M.D., 1999. Orientation and magnitude of in situ stress to 6.5 km depth in the Baltic Shield. Int. J. Rock Mech. Min. Sci. 36, 169–190.

Lund, B., Schmidt, P., Shomali, Z.H., Roth, M., 2021. The modern Swedish national seismic network: two decades of intraplate microseismic observation. Seismol. Res. Lett. 92, 1747–1758. https://doi.org/10.1785/0220020435.

Luthi, S.M., Souhaité, P., 1990. Fracture apertures from electrical borehole scans. Geophysics 55, 821–833.

Lyngsie, S.B., Thybo, H., 2007. A new tectonic model for the Laurentia–Avalonia–Baltica suture in the North Sea: a case study along MONA LISA profile 3. Tectonophysics 429, 201–227. https://doi.org/10.1016/j.tecto.2006.09.017.

Müllern, C.-F., 1978. Den prekambriska berggrunden. In: Gustafsson, O. (Ed.), Beskrivning av hydrogeologiska kartbladet Trelleborg NO/Malmö NO. Sveriges geologiska undersökning Ag, Beskrivning av hydrogeologiska kartbladet Trelleborg NO/Malmö NO. Sveriges geologiska undersökning Ag, 6, pp. 8–11.

Meet, 2019. Deliverable D3.2. 1D/2D DFN Models of borehole fractures and hydraulic circulation simulations. H2020 Grant Agreement N° 792037, www.meet-h2020.com/wp-content/uploads/2020/07/MEET_Deliverable_D3.2_25042019_VF.pdf.

Mogensen, T.E., 1994. Palaeozoic structural development along the Tornquist Zone, Kattegat, Denmark. Tectonophysics 240, 191–214.

Mogensen, T.E., 1995. Triassic and Jurassic structural development along the Tornquist Zone, Denmark. Tectonophysics 252, 19–220.

Muhamad, H., Juhlin, C., Lehnert, O., Meinhold, G., Andersson, M., Juanatey Garcia, M., Malehmir, A., 2015. Analysis of borehole geophysical data from the Mora area of the Siljan Ring impact structure, central Sweden. J. Appl. Geophys. 115, 183–196.

Näslund, J.-O., Jansson, P., Fastook, J.L., Johnson, J., Andersson, L., 2005. Detailed spatially distributed geothermal heat-flow data for modeling of basal temperatures and meltwater production beneath the Fennoscandian ice sheet. Ann. Glaciol. 40, 95–101.

Reinecker, J., Gutmanis, J., Foxford, A., Cotton, L., Dalby, C., Law, R., 2021. Geothermal exploration and reservoir modelling of the Unit Downs deep geothermal project, Cornwall (UK). Geothermics 97. https://doi.org/10.1016/j. geothermics.2021.102226.

Rogers, S., Elmo, D., Webb, G., Catalan, A., 2015. Volumetric fracture intensity measurement for improved rock mass characterisation and fragmentation assessment in block caving operations. Rock Mech. Rock Eng. 48, 633–649.

Rosberg, J.-E., Erlström, M., 2019. Evaluation of the Lund deep geothermal exploration project in the Romeleåsen Fault Zone, South Sweden: a case study. Geotherm. Energy 7 (10). https://doi.org/10.1186/s40517-019-0126-7.

Rosberg, J.-E., Erlström, M., 2021. Evaluation of deep geothermal exploration drillings in the crystalline basement of the Fennoscandian Shield Border Zone in south Sweden. Geotherm. Energy 9, 20. https://doi.org/10.1186/s40517-021-00203-1.

Rögnvaldsson, S.Th, Slunga, R., 1993. Routine fault plane solutions for local and regional networks: a test with synthetic data. Bull. Seismol. Soc. Am. 11, 1232–1247.

Sivhed, U., Wikman, H., Erlström, M., 1999. Beskrivning till berggrundskartorna 1C Trelleborg NV, NO, 2C Malmö SV, SO, NV, NO (in Swedish with an English summary). Sveriges geologiska Undersökning 198, 1–143. Af 191–194, 196, 198.

Sivhed, U., 1991. A pre-quaternary, post-Palaeozoic erosional channel deformed by strike-slip faulting, Scania, southern Sweden. Geologiska Föreningens i Stockholm Förhandlingar 113, 139–143.

SKB, 2009. Site Description of Laxemar at Completion of the Site Investigation Phase SDM-Site Laxemar, p. 637. SKB report TR 09-01.

Slunga, R., 1981. Earthquake source mechanism determination by use of body-wave amplitudes - an application to Swedish earthquakes. Bull. Seismol. Soc. Am. 71, 25–35.

SNSN, 1904. Swedish National Seismic Network. Uppsala University, Uppsala, Sweden. https://doi.org/10.18159/SNSN. Other/Seismic network.

Stephens, M.B., Wahlgren, C.-H., 2020. Chapter 15: polyphase (1.9–1.8, 1.5–1.4 and 1.0–0.9 Ga) deformation and metamorphism of proterozoic (1.9-1.2 Ga) continental crust Eastern segment, Sveconorwegian orogen. In: Stephens, M.-B., Bergman Weihed, J. (Eds.), Sweden Lithotectonic Framework, Tectonic Evolution and Mineral Resources, Sweden Lithotectonic Framework, Tectonic Evolution and Mineral Resources, 50. Geological Society Memoir, pp. 351–396.

Stephens, M., Follin, S., Petersson, J., Isaksson, H., Juhlin, C., Simenonov, A., 2015. Review of the deterministic modelling of deformation zones and fracture domains at the site proposed for a spent nuclear fuel repository, Sweden, and consequences of structural anisotropy. Tectonophysics 653, 68–94.

Tanner, B., Meissner, R., 1996. Caledonian deformation upon southwest Baltica and its tectonic implications: alternatives and consequences. Tectonics 15, 803–812.

Thomas, S.A., Deeks, N.R., 1994. Seismic evidence for inversion tectonics in the strike-slip regime of the Tornquist Zone, Southern Baltic Sea. Zeitschrift fur geologisches Wissenschaften 22, 33–45.

Thybo, H., 1990. A seismic velocity model along the EGT profile from the North German Basin into the Baltic Shield. In: Freeman, R., Giese, P., Mueller, St. (Eds.), The European Geotraverse: Integrative Studies. European Scientific Foundations, Strasbourg, pp. 99–108.

Thybo, H., 1997. Geophysical characteristics of the Tornquist Fan area, northwest Trans-European Suture Zone: indication of late Carboniferous to early Permian dextral transtension. Geol. Mag. 134, 597–606.

Thybo, H., 2000. Crustal structure and tectonic evolution of the Tornquist Fan region as revealed by geophysical methods. Bull. Geol. Soc. Den. 46, 145–160.

Ulmius, J., Möller, C., Page, L., Johansson, L., Ganerod, M., 2018. The eastern boundary of Sveconorwegian reworking in the Baltic Shield defined by 40Ar/39Ar geochronology across the southernmost Sveconorwegian Province. Precambrian Res. 307, 201–217.

Veikkolainen, T., Kukkonen, I.T., Tiira, T., 2017. Heat flow, seismic cut-off depth and thermal modeling of the Fennoscandian Shield. Geophys. J. Int. 211, 1414–1427.

Wallroth, T., Eliasson, T., Sundquist, U., 1999. Hot dry rock research experiments at Fjällbacka, Sweden. Geothermics 28, 617–625.

Zimmermann, G., Alexander, K., Burkhardt, H., 2000. Hydraulic pathways in the crystalline rock in KTB. Geophys. J. Int. 142, 4–14.

Zoback, M,D, 2007. In: Reservoir Geomechanics. Cambridge University Press, Cambridge, UK.